

Ballistic-hydrodynamic phase transition in flow of two-dimensional electrons

A. N. Afanasiev, P. S. Alekseev, A. A. Greshnov, and M. A. Semina
Ioffe Institute, St. Petersburg 194021, Russia
(Dated: June 22, 2021)

Phase transitions are characterized by a sharp change in the type of dynamics of microparticles, and their description usually requires quantum mechanics. Recently, a peculiar type of conductors was discovered in which two-dimensional (2D) electrons form a viscous fluid. In this work we reveal that such electron fluid in high-quality samples can be formed from ballistic electrons via a phase transition. For this purpose, we theoretically study the evolution of a ballistic flow of 2D weakly interacting electrons with an increase of magnetic field and trace an emergence of a fluid fraction at a certain critical field. Such restructuring of the flow manifests itself in a kink in magnetic-field dependencies of the longitudinal and the Hall resistances. It is remarkable that the studied phase transition has a classical-mechanical origin and is determined by both the ballistic size effects and the electron-electron scattering. Our analysis shows that this effect was apparently observed in the recent transport experiments on 2D electrons in graphene and high-mobility GaAs quantum wells.

1. Introduction. Frequent electron-electron collisions in high-quality conductors can lead to realization of the hydrodynamic regime of charge transport [1]. This regime was recently reported for high-quality graphene [2–6], Weyl semimetals [7, 8], and GaAs quantum wells [9–23]. Formation of the electron fluid was detected by a specific dependence of the resistance on the sample width [7]; by observation of the negative nonlocal resistance [2, 3, 15, 22], the giant negative magnetoresistance [8–14, 16, 17, 23], and the magnetic resonance at double cyclotron frequency [18–21].

Much attention was paid to the transition between the hydrodynamic and non-hydrodynamic regimes of electron transport. In Refs. [5, 6] precise measurements of profiles of the Hall electric field and the current density of 2D electron flow in graphene stripes were performed. This allowed to detect the Ohmic, the hydrodynamic, and the ballistic flows at varying temperature, electron density and magnetic field. In particular, a peculiar non-monotonic magnetoresistance reflecting the ballistic and the hydrodynamic transport regimes was observed [5, 6]. Similar magnetoresistance was detected in long samples of high-quality GaAs quantum wells [14, 16], that, apparently, also evidences the ballistic-hydrodynamic transition. In Refs. [22, 23] the transitions from the ballistic to the hydrodynamic regimes in GaAs quantum wells with changing of the sample geometry, temperature and magnetic field were vividly demonstrated.

A theory of 2D electron flow in samples with macroscopic obstacles was constructed in Ref. [24]. In the absence of magnetic field, the ballistic-hydrodynamic transition occurs in such system with changing the interparticle scattering rate and has the type of a smooth crossover. A numerical theory of the ballistic-Ohmic transition and the hydrodynamic transport for 2D electrons in stripes in a perpendicular magnetic field was developed in Ref. [25]. At weak interparticle and disorder scattering rates, the longitudinal and the Hall resistances of a stripe as functions of magnetic field B exhibit kinks at the field $B = B_c$

above which the diameter of the electron cyclotron orbit, $2R_c$, becomes smaller than the sample width, W . In Ref. [26] the same system was theoretically studied in more details. It was shown that an increase of the curvature of the Hall electric field characterizes the transition from the ballistic to the hydrodynamic regimes.

In this Letter, we demonstrate that the hydrodynamic regime of transport of 2D electrons in high-quality stripes is formed from the ballistic regime via a genuine phase transition with the increase of magnetic field B . For this purpose, first, we reveal that in the lower vicinity of the critical field, $0 < B_c - B \ll B_c$, the momentum relaxation due to collisions of electrons with the stripe edges becomes strongly suppressed due to the ballistic size effects, thus even weak electron-electron scattering begins to be important for the flow formation. Second, we show that in the upper vicinity of B_c , $0 < B - B_c \ll B_c$, the emerging “central” electrons, which are not scattered at the edges, critically change the type of the electron distribution and become the nucleus of a collectivized fluid phase. We develop a mean field model based on the classical kinetic equation to describe these critical transport regimes of the ballistic-hydrodynamic phase transition. Our analysis of the results of experiments [5, 6] evidences that formation of the hydrodynamic regime from the ballistic one was realized in them via such phase transition.

Using the developed approach, we also obtain new results on the ballistic transport in stripes at low magnetic fields, $B \ll B_c$. In particular, we show that the interplay of the ballistic effects and the interparticle scattering induces a strongly nonuniform electron flow and a non-trivial character of the Hall effect.

2. Ballistic regime. We consider a flow of 2D degenerate electrons in a long sample with rough edges in a perpendicular magnetic field \mathbf{B} (see Fig. 1). Electrons are diffusively scattered on the rough sample edges leading to momentum relaxation. In the bulk of the sample, electrons collide with each other and their total momentum is conserved. We assume that the rate γ of the electron-

electron scattering is weak: $W \ll l$, where $l = v_F/\gamma$ is the mean free path and v_F is the Fermi velocity. We describe the transport in this system by the non-equilibrium part $\delta f(y, \varphi, \varepsilon)$ of the distribution function $f = f_F + \delta f$ determined by the linearized kinetic equation:

$$v_F \cos \varphi \frac{\partial \delta f}{\partial y} + \frac{e}{m} \mathbf{E} \cdot \frac{\partial f_F}{\partial \mathbf{v}} - \omega_c \frac{\partial \delta f}{\partial \varphi} = \text{St}[\delta f] \quad (1)$$

with the diffusive boundary conditions at $y = \pm W/2$. Here ε is the electron energy, φ is the angle of the electron velocity $\mathbf{v}/v_F = (\cos \varphi, \sin \varphi)$, f_F is the Fermi distribution, $\omega_c = v_F/R_c$ is the cyclotron frequency, e and m are the electron charge and mass, $\mathbf{E} = \mathbf{E}_0 + \mathbf{E}_H$ is the total electric field, \mathbf{E}_0 is the applied field, \mathbf{E}_H is the Hall field, $\text{St}[\delta f] = -\gamma(\delta f - \hat{P}[\delta f])$ is the simplified interparticle collision operator, in which \hat{P} is the projector onto the zeroth and first harmonics of δf by φ .

At the magnetic fields B below the critical field, $B < B_c$, when $2R_c > W$, each electron is predominantly scattered at the edges. The transport is ballistic in almost all such B , and the interparticle collisions can constrain the time which electrons spend on the ballistic trajectories. Our analysis [27] based on Eq. (1) shows that the ballistic regime has a fine structure, namely, it is divided into the three subregimes.

In the first ballistic subregime of low fields $B \ll B_c(W/l)^2$, the electron trajectories are almost straight. Their maximum length is limited by the interparticle scattering length l . This subregime was studied in Refs. [28, 29] and in this work [27]. Depending on the arrangement of trajectories, electrons are divided on the two groups: the “traveling electrons” which, after scattering on an edge, reach the other edge or scatter in the bulk, and the “skipping electrons” which return to the same edge after scattering on it [see Fig. 1(a,b)]. Most of electrons belong to the first type. Electrons of the second type are located in the edge vicinities, $W/2 - |y| \lesssim l^2/R_c$, and their velocity angles are $\varphi \approx \pm\pi/2$.

In the central part of the sample, $W/2 - |y| \gg l^2/R_c$, the Hall electric field $E_H(y)$ is related to the dynamics of the “traveling electrons” [27]. The resulting local Hall resistance, $\varrho_{xy}(y) = E_H(y)/j(y)$, turns out to be one half of the Hall resistance of macroscopic Ohmic samples [29]:

$$\varrho_{xy} = R_H^{(0)} B/2, \quad R_H^{(0)} = 1/(n_0 e c), \quad (2)$$

where $j(y)$ is the current density, n_0 is the electron density, and c is the velocity of light. In Ref. [29] this result was obtained from a straightforward solution of kinetic equation (1). In this work we reveal [27] the physical essence of result (2). Namely, the value E_H yielding Eq. (2) corresponds to the balance of the Hall force eE_H and the component of the Lorentz force $\Delta F_{L,y}(t) = eBa_x t/c$, averaged over all the traveling electrons in the region $W/2 - |y| \gg l^2/R_c$. Here $a_x = eE_0/m$ is the acceleration of electrons by the field E_0 and $t = t(y, \varphi)$ is the time passed since the scattering at the edge.

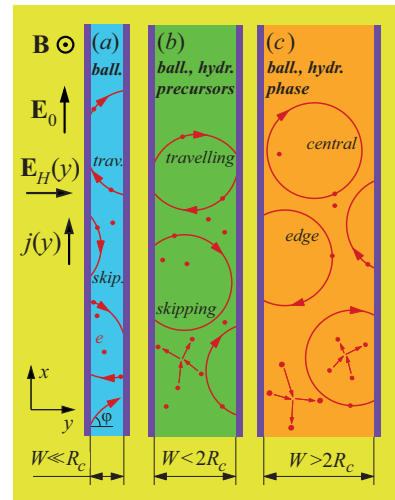


FIG. 1. Two-dimensional electrons in a long sample at low, $W \ll R_c$ (a); intermediate, $W \sim R_c$, $W < 2R_c$ (b); and moderately high, $W \sim R_c$, $W > 2R_c$ (c) magnetic fields. The ballistic-hydrodynamic phase transition occurs at the critical field B_c corresponding to $2R_c = W$. In its lower vicinity, $0 < B_c - B \ll B_c$, electrons moving along the skipping orbits close to complete cyclotron circles undergo slow momentum relaxation. They are precursors of hydrodynamic flow. Above the critical point, $B > B_c$, a group of the central electrons appears those do not collide with the edges, representing a nucleus of the hydrodynamic fluid phase.

In the vicinities of the edges, $W/2 - |y| \lesssim l^2/R_c$, the Hall field $E_H(y)$ and the current density $j(y)$ are strongly affected by the skipping electrons [see Fig. 2(b)]. The resulting values of $E_H(y)$ and $j(y)$ determine the resistances ϱ_{xx} and ϱ_{xy} of the whole sample, provided it is sufficiently long and straight [27].

In the second ballistic subregime, $B_c(W/l)^2 \ll B \ll B_c$, electron trajectories become substantially bent. Their maximal length is now limited by their geometry. This subregime was studied in Refs. [25] by numeric solution of Eq. (1) and in Refs. [26] by its analytical solution accounting only for the departure term $-\gamma \delta f$ in the operator St . The resulting longitudinal and Hall resistances exhibit the singular behavior, $\varrho_{xx,xy}(B) \sim 1/\ln(\sqrt{R_c/W})$, originating from the shortening of the longest ballistic trajectories with the increase of B [27].

In the third ballistic subregime, $B_c W/l \ll B_c - B \lesssim B_c$, the number of the skipping electrons becomes relatively large: comparable with or even greater than the number of traveling ones [see Fig. 1(b)]. To our knowledge this subregime has not been noticed and studied yet. In order to satisfy the condition $j_y = 0$ of the absence of the transverse current, the $\mathbf{E}_0 \times \mathbf{B}$ -drift contribution related to all electrons, $j_y^{(0)} = n_0 e c E_0/B$, is compensated by the excess and the deficiency of non-equilibrium traveling electrons with $v_y(t) > 0$ and with $v_y(t) < 0$. Non-equilibrium skipping electrons do not compensate

$j_y^{(0)}$, as $v_y(t) > 0$ and $v_y(t) < 0$ symmetrically for each skipping trajectory. The diffusive reflection of electrons from the edges occurs with equal probabilities for all φ . Thus, at $2R_c/W - 1 \ll 1$, when the skipping electrons dominate, the whole electron density strongly increases (as compared with the case $2R_c/W - 1 \sim 1$) in order to compensate $j_y^{(0)}$ by the relatively small part of the traveling electrons.

This dynamics is described by the distribution [27]:

$$\delta f(y, \varphi, \varepsilon) = [E_0/(\omega_c u)] \chi(y, \varphi) f'_F(\varepsilon), \quad (3)$$

where the behavior of the factor χ , $\chi(y, \varphi) \approx 1$ at $-\pi + \varphi_- < \varphi < \varphi_+$ and $\chi(y, \varphi) \approx -1$ at $\varphi_+ < \varphi < \pi + \varphi_-$, reflects the domination of the skipping electrons {here $\varphi_{\pm}(y) = \arcsin[1 - (W/2 \pm y)/R_c]$. The small parameter $u(B) = (2/\pi)(2 - W/R_c) \ll 1$ in Eq. (3) shows how close is B to the critical field B_c . The resulting current density and the Hall field in the main order by u take the form:

$$j(y) = 2r(y)j_0/(\pi u), \quad E_H(y) = 2E_0/[\pi r(y)u], \quad (4)$$

where $j_0 = n_0 e^2 E_0 W / (v_F m)$ and $r(y) = \sqrt{1 - (y/R_c)^2}$. The magnitudes of $j(y)$ and $E_H(y)$ rapidly increase as B approaches B_c . The averaged resistances $\varrho_{xx} = E_0/\langle j(y) \rangle$ and $\varrho_{xy} = \langle E_H(y) \rangle / \langle j(y) \rangle$ determined by δf after Eq. (3) in the two main orders by \sqrt{u} are:

$$\varrho_{xx}(B) = 2\varrho_0 u, \quad \varrho_{xy}(B) = R_H^{(0)} B F(u), \quad (5)$$

where $\varrho_0 = E_0/j_0$ and $F(u) = 1 - \sqrt{u/\pi}$. The vanishing of ϱ_{xx} as $\sim u$ reflects the transitional character of the ballistic electron dynamics at $B \rightarrow B_c$ [see Fig. 1(b)].

The evolution of $j(y)$ and $E_H(y)$ in the ballistic subregimes with the increase of B are shown in Figs. 2(a-e).

3. Phase transition. At the fields B in the upper and the lower vicinities of B_c , $|B - B_c| \ll B_c$, most of electrons are the ‘‘edge electrons’’ those move along the skipping trajectories those hit one of the edges. In the upper vicinity, when $W > 2R_c$, a small group of the ‘‘central electrons’’ arises those never touch the edges [Fig. 1(c)].

In the nearest lower vicinity of B_c , $0 < B_c - B \lesssim B_c W/l$, the imbalance in densities of the left-edge and the right-edge skipping electrons increases dramatically, as ballistic distribution function (3) and values (4) diverge by $u \rightarrow 0$ at $W/l \rightarrow 0$. Therefore the electron dynamics at such B is to be controlled not only by their scattering on the edges, but also by interparticle collisions.

To describe such semiballistic flow, first, we calculate [27] the trial distribution function, similar to purely ballistic function (3), but additionally accounting for the departure term $-\gamma \delta f$ in the operator St in Eq. (1):

$$\delta f_d(y, \varphi, \varepsilon) = \frac{E_0/\omega_c}{u + W/l} \chi(y, \varphi) f'_F(\varepsilon). \quad (6)$$

The averaged current density and the Hall field corresponding to δf_d rapidly increase at $B \rightarrow B_c$ up to the

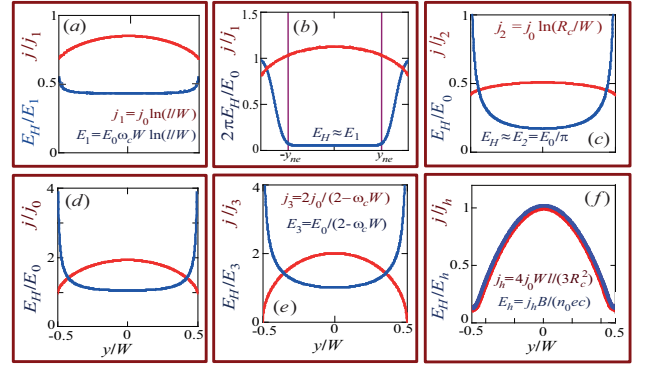


FIG. 2. Current density $j(y)$ and Hall electric field $E_H(y)$ at various magnetic fields B : (a) the first ballistic subregime, in the limit $B \rightarrow 0$ [only the flow in the central part of the sample, $W/2 - |y| \gg l^2/R_c$, is shown]; (b) the middle part of the first ballistic subregime, $R_c \gg l^2/W$ [schematically; violet lines depict the boundaries of the near-edge regions where skipping electrons propagate, $y_{nc} \approx \pm(W/2 - l^2/R_c)$]; (c) the second ballistic subregime, $W \ll R_c \ll l^2/W$; (d) the middle part of the third ballistic subregime, $0 < 2R_c/W - 1 \sim 1$; (e) the upper part of the third ballistic subregime near the critical field, $W/l \ll 2R_c/W - 1 \ll 1$; and (f) the hydrodynamic regime with a Poiseuille flow, $W \gg R_c$ (schematically).

values limited by the slow scattering rate $\gamma = v_F/l$:

$$j_d = \frac{j_0/2}{u + W/l}, \quad E_{H,d} = \frac{E_0 F(u)}{u + W/l}. \quad (7)$$

Second, to describe the flow at $0 < B_c - B \lesssim B_c W/l$, we need to account for the effect of the arrival term $\gamma \hat{P}[\delta f]$ in Eq. (1). Indeed, the departure term $-\gamma \delta f$ dominates in the first ballistic subregime [28], both the departure and the arrival terms are relatively small in the second and the third ballistic subregimes [26, 27], whereas in a well-formed hydrodynamic flow at $W \gg R_c$ they are close one to other [28]. An estimate shows that for function f_d (6) at $0 < 2R_c - W \lesssim W^2/l$ these two terms have the values of the same order of magnitude. In this connection, we propose a mean field model based on the approximation of the arrival term $\gamma \hat{P}[\delta f]$ [27] by its averaged by y value, whose main part is: $\gamma \sin \varphi j / (n_0/m)$. After this substitution, the external field E_0 in kinetic equation (1) is changed on the effective one: $\tilde{E}_0 = E_0 + \gamma j / (n_0/m)$. As a result, the self-consistent distribution f and averaged current density j are given by semiballistic formulas (6) and (7) with $E_0 \rightarrow \tilde{E}_0$. For j we obtain:

$$j = \frac{1}{2} \frac{j_0 + j W/l}{u + W/l} \quad (8)$$

This mean-field-type equation accounts for the redistribution of momentum between the skipping electrons in their collisions with each other, while formulas (6) and (7) imply the relaxation of momentum in scattering of electrons in the bulk. The solution of Eq. (8)

is $j = j_0/[2u + W/l]$. To find the Hall field near the critical point, we should substitute the renormalization $E_0 \rightarrow \tilde{E}_0$ in the semiballistic value $E_{H,d}$ (7), that yields: $E_H = E_0 F(u)/[u + W/(2l)]$.

In the upper vicinity of the transition point, $0 < B - B_c \ll B_c$, when the relative density of the central electrons is small, $\alpha_c = (W - 2R_c)/W \ll 1$, each edge electron is still scattered predominantly on the edges and on the other edge electrons. Similarly as for the flow in the lower vicinity of B_c , $0 < B_c - B \ll B_c$ the distribution function of these electrons, δf_e , is given by a formula based on the semiballistic distribution δf_d (6). Therefore the departure and the arrival terms of St in Eq. (1) with this δf_e are also of the same order of magnitude. To account the arrival term $\gamma P[\delta f]$, we again substitute it by its averaged value, which is mainly proportional to the averaged current $j = j_e + j_c$ corresponding to $\delta f = \delta f_e + \delta f_c$. As a result, the function δf_e is given by Eq. (6) at $u = 0$ with the sample width W changed on the width $\tilde{W} = 2R_c$ of the subregion with the edge electrons and the renormalized electric field $E_0 \rightarrow \tilde{E}_0 = E_0 + \gamma(j_e + j_c)/(n_0/m)$. Correspondingly, for the current component j_e we should use Eq. (8) at $u = 0$ with $j = j_e + j_c$ and the density factor $\alpha_e = \tilde{W}/W$.

All the central electrons have almost coinciding trajectories and are scattered mainly by the edge ones [see Fig. 1(c)]. Thus the flow of the central electrons is similar to an Ohmic one, and their component j_c is given by the Drude formula with the density factor α_c and the same \tilde{E}_0 . In the distribution of the central electron δf_c the first angular harmonic dominate, unlike the semiballistic function δf_b (6), which is discontinuous in φ and, thus, contains many comparable harmonics by φ [27].

We arrive the mean field equations for j_e and j_c [27]:

$$\begin{aligned} j_e &= \alpha_e (j_{cr} + j_e + j_c)/2, \\ j_c &= \alpha_c (j_{cr} + j_e + j_c), \end{aligned} \quad (9)$$

where $j_{cr} = j_0 l/W$. These equations are similar by their meaning to the one-component equation (8), but accounts for the appearance at $B > B_c$ of the two electron species. Solution of (9) yields: $j = (1 + 2\alpha_c)j_{tr}$.

The Hall field is also related to the edge and the central electrons: $E_H = E_{H,e} + E_{H,c}$. The first term is calculated by Eq. (7) at $u = 0$ with the factor α_e and the substitutions $E_0 \rightarrow \tilde{E}_0$ and $W \rightarrow \tilde{W}$. According to the Ohmic-like form of the distribution δf_c , the term $E_{H,c}$ is given by the Drude formula $E_{H,c} = \omega_c j_c/(n_0/m)$. As a result, we obtain: $E_H = (1 + 2\alpha_c)(l/R_c)E_0$.

The described change in electron dynamics above and below the critical field is reflected in kinks in the obtained magnetic dependencies $j(B)$ and $E_H(B)$. Next, for ρ_{xx} in the main orders by $|b| \ll 1$ and $W/l \ll 1$ we obtain [27]:

$$\frac{\rho_{xx}(B)}{\rho_{cr}} = 1 - b \begin{cases} 8l/(\pi W), & b < 0, |b| \ll 1 \\ 2, & 0 < b \ll 1 \end{cases}. \quad (10)$$

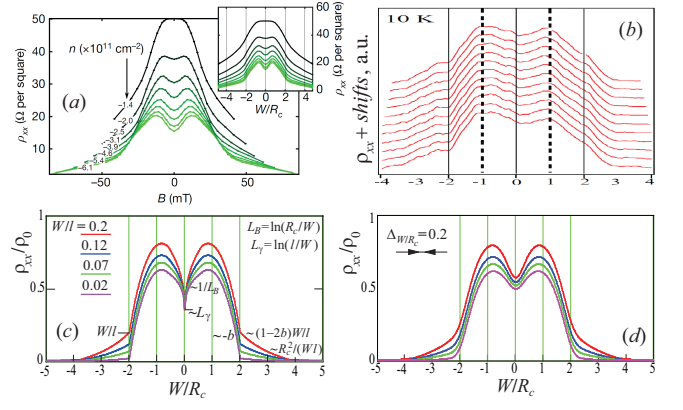


FIG. 3. Longitudinal resistance ρ_{xx} of long samples as a function of magnetic field $B \propto W/R_c$. Panels (a) and (b) present experimental results for graphene stripes and are taken from Refs. [5] and [6], respectively. Different curves correspond to varying 2D electron densities, controlled by the gate voltages. Distortions of the curves in panel (b), asymmetric in B , can be due to some contribution from the Hall resistance ρ_{xy} in the measured data. (c): Results of our theory for several the interparticle scattering rates γ . In panel (d) we plot the curves from panel (c), smoothed by convolution with a Gaussian weight function $G_\Delta(B)$ with the width $\Delta W/R_c$, that simulates contribution from sample corners, several sections of a long sample with varying widths, and other imperfections.

where $\rho_{cr} = E_0/j_{cr}$ and $b = (B - B_c)/B_c$. For the Hall resistance $\rho_{xy}(B)$ in the main order by W/l and the two first orders by $\sqrt{|b|}$ we obtain the same result as in Eqs. (5) at $b < 0$, while at $b > 0$ the above formulas for j and E_H yield: $\rho_{xy}(B) \equiv R_H^{(0)} B$. The kinks in the obtained longitudinal and the Hall resistances at $B = B_c$ evidence that the formation of the hydrodynamic flow from the ballistic one is realized via a phase transition.

With the increase of B and α_c , the collisions between the central electrons become important, therefore j_c becomes non-uniform by y . The hydrodynamic-ballistic flow at $\alpha_c \sim 1$ was numerically studied in Refs. [25, 26]. At $\alpha_c \gg 1$ the central electrons dominate everywhere except the edges vicinities, $W/2 - |y| \sim R_c$, and the Poiseuille flow $j_c(y) \sim (W/2)^2 - y^2$ is formed [see Fig. 2(f)]. The resulting resistance ρ_{xx} is determined by the viscosity: $\rho_{xx} \sim \eta_{xx}/W^2$, $\eta_{xx} \sim \gamma/\omega_c^2$, while the Hall resistance ρ_{xy} is close to $\rho_{xy}^{(0)} = R_H^{(0)} B$ [17].

In Fig. 3 we compare the results of experiments [5, 6] on 2D electron transport in high-quality graphene stripes with our theoretical results. Both the theoretical and the experimental resistances ρ_{xx} have similar profiles, including the minimum at $W/R_c \ll 1$, the maximum at $W/R_c \sim 1$, and the kink at $W/R_c = 2$. Convolution of the calculated dependencies $\rho_{xx}(B)$ with a weight function $G_\Delta(B)$, simulating the imperfection of the sample, leads to a very good agreement of the shapes of the observed and calculated curves [compare (a) and (d)]. In

Supplementary material [27] we also compare our results with preceding theories [25, 26] and other related experiments [9–11, 16]. Numerical solution [25] of Eq. (1) for the stripes in which the scattering on disorder dominates leads to the dependencies $\rho_{xx,xy}(B)$ almost identical to the ones calculated within our theory based on Eq. (1) with $St = St_{dis}$ (see details in [27]). Our analytical results for the second ballistic subregime coincide with the ones obtained in Ref. [26]. The longitudinal and Hall resistances observed in Ref. [16] in long high-quality samples of GaAs quantum wells are in a good agreement with the calculated dependencies $\rho_{xx,xy}(B)$ [27].

4. *Conclusion.* The phase transition between the ballistic and the hydrodynamic regimes of transport has been revealed and studied for 2D electrons in long samples in a magnetic field. Analysis of magnetotransport experiments [5, 6, 16] on high-quality stripes of graphene and GaAs quantum well shows that this transition was apparently observed in them.

Similar magnetic-field-induced ballistic-hydrodynamic phase transitions may be possibly realized also in materials with other geometries of 2D electron flows [27].

We thank A. I. Chugunov, L. E. Golub, and A. V. Shumilin for fruitful discussions. The study was supported by the Russian Foundation for Basic Research (Grant No. 19-02-00999) and by the Foundation for the Advancement of Theoretical Physics and Mathematics "BASIS".

-
- [1] R. N. Gurzhi, *Sov. Phys. Uspekhi* **11**, 255 (1968).
- [2] D. A. Bandurin, I. Torre, R. K. Kumar, M. Ben Shalom, A. Tomadin, A. Principi, G. H. Auton, E. Khestanova, K. S. Novoselov, I. V. Grigorieva, L. A. Ponomarenko, A. K. Geim, and M. Polini, *Science* **351**, 1055 (2016).
- [3] L. Levitov and G. Falkovich, *Nature Physics* **12**, 672 (2016).
- [4] A. I. Berdyugin, S. G. Xu, F. M. D. Pellegrino, R. Krishna Kumar, A. Principi, I. Torre, M. Ben Shalom, T. Taniguchi, K. Watanabe, I. V. Grigorieva, M. Polini, A. K. Geim, and D. A. Bandurin, *Science* **364**, 162 (2019).
- [5] J. A. Sulpizio, L. Ella, A. Rozen, J. Birkbeck, D. J. Perello, D. Dutta, M. Ben-Shalom, T. Taniguchi, K. Watanabe, T. Holder, R. Queiroz, A. Principi, A. Stern, T. Scaffidi, A. K. Geim, and S. Ilani, *Nature* **576**, 75 (2019).
- [6] M. J. H. Ku, T. X. Zhou, Q. Li, Y. J. Shin, J. K. Shi, C. Burch, L. E. Anderson, A. T. Pierce, Y. Xie, A. Hamo, U. Vool, H. Zhang, F. Casola, T. Taniguchi, K. Watanabe, M. M. Fogler, P. Kim, A. Yacoby, and R. L. Walsworth, *Nature* **583**, 537 (2019).
- [7] P. J. W. Moll, P. Kushwaha, N. Nandi, B. Schmidt, and A. P. Mackenzie, *Science* **351**, 1061 (2016).
- [8] J. Gooth, F. Menges, N. Kumar, V. Süß, C. Shekhar, Y. Sun, U. Drechsler, R. Zierold, C. Felser, and B. Gotsmann, *Nature Communications* **9**, 4093 (2018).
- [9] L. Bockhorn, P. Barthold, D. Schuh, W. Wegscheider, and R. J. Haug, *Phys. Rev. B* **83**, 113301 (2011).
- [10] A. T. Hatke, M. A. Zudov, J. L. Reno, L. N. Pfeiffer, and K. W. West, *Phys. Rev. B* **85**, 081304 (2012).
- [11] R. G. Mani, A. Kriisa, and W. Wegscheider, *Scientific Reports* **3**, 2747 (2013).
- [12] Q. Shi, P. D. Martin, Q. A. Ebner, M. A. Zudov, L. N. Pfeiffer, and K. W. West, *Phys. Rev. B* **89**, 201301 (2014).
- [13] L. Bockhorn, I. V. Gornyi, D. Schuh, C. Reichl, W. Wegscheider, and R. J. Haug, *Phys. Rev. B* **90**, 165434 (2014).
- [14] G. M. Gusev, A. D. Levin, E. V. Levinson, and A. K. Bakarov, *AIP Advances* **8**, 025318 (2018).
- [15] A. D. Levin, G. M. Gusev, E. V. Levinson, Z. D. Kvon, and A. K. Bakarov, *Phys. Rev. B* **97**, 245308 (2018).
- [16] G. M. Gusev, A. D. Levin, E. V. Levinson, and A. K. Bakarov, *Phys. Rev. B* **98**, 161303 (2018).
- [17] P. S. Alekseev, *Phys. Rev. Lett.* **117**, 166601 (2016).
- [18] Y. Dai, R. R. Du, L. N. Pfeiffer, and K. W. West, *Phys. Rev. Lett.* **105**, 246802 (2010).
- [19] A. T. Hatke, M. A. Zudov, L. N. Pfeiffer, and K. W. West, *Phys. Rev. B* **83**, 121301 (2011).
- [20] M. Białek, J. Lusakowski, M. Czapkiewicz, J. Wróbel, and V. Umansky, *Phys. Rev. B* **91**, 045437 (2015).
- [21] P. S. Alekseev and A. P. Alekseeva, *Phys. Rev. Lett.* **123**, 236801 (2019).
- [22] A. C. Keser, D. Q. Wang, O. Klochan, D. Y. H. Ho, O. A. Tkachenko, V. A. Tkachenko, D. Culcer, S. Adam, I. Farrer, D. A. Ritchie, O. P. Sushkov, and A. R. Hamilton, (2021), [arXiv:2103.09463 \[cond-mat.mes-hall\]](https://arxiv.org/abs/2103.09463).
- [23] A. Gupta, J. J. Heremans, G. Kataria, M. Chandra, S. Fallahi, G. C. Gardner, and M. J. Manfra, *Phys. Rev. Lett.* **126**, 076803 (2021).
- [24] H. Guo, E. Ilseven, G. Falkovich, and L. S. Levitov, *PNAS* **114**, 3068 (2017).
- [25] T. Scaffidi, N. Nandi, B. Schmidt, A. P. Mackenzie, and J. E. Moore, *Phys. Rev. Lett.* **118**, 226601 (2017).
- [26] T. Holder, R. Queiroz, T. Scaffidi, N. Silberstein, A. Rozen, J. A. Sulpizio, L. Ella, S. Ilani, and A. Stern, *Phys. Rev. B* **100**, 245305 (2019).
- [27] See Supplementary material below, containing additional references [30–35], for the details of the theory and of the comparison of its results with preceding works.
- [28] P. S. Alekseev and M. A. Semina, *Phys. Rev. B* **98**, 165412 (2018).
- [29] P. S. Alekseev and M. A. Semina, *Phys. Rev. B* **100**, 125419 (2019).
- [30] P. S. Alekseev and A. P. Dmitriev, *Phys. Rev. B* **102**, 241409 (2020).
- [31] C. Beenakker and H. van Houten, in *Semiconductor Heterostructures and Nanostructures*, Solid State Physics, Vol. 44, edited by H. Ehrenreich and D. Turnbull (Academic Press, 1991) pp. 1–228.
- [32] E. M. Baskin, L. N. Magarill, and M. V. Entin, *Zh. Exp. Teor. Fiz.* **75**, 723 (1978).
- [33] A. V. Bobylev, F. A. Maaø, A. Hansen, and E. H. Hauge, *Phys. Rev. Lett.* **75**, 197 (1995).
- [34] A. Dmitriev, M. Dyakonov, and R. Jullien, *Phys. Rev. B* **64**, 233321 (2001).
- [35] Y. M. Beltukov and M. I. Dyakonov, *Phys. Rev. Lett.* **116**, 176801 (2016).

Supplementary material to “Ballistic-hydrodynamic phase transition in flow of two-dimensional electrons”

A. N. Afanasiev, P. S. Alekseev, A. A. Greshnov, and M. A. Semina

Ioffe Institute, St. Petersburg 194021, Russia

Here we present the details of our theoretical model (Sec. 1), the solution of its equations for the ballistic regime and the derivation of the properties of the resulting ballistic flow (Sec. 2), and the detailed report on the construction of the mean field theory for the ballistic-hydrodynamic phase transition (Sec. 3). We also compare in detail our results with the results of preceding theoretical and experimental studies (Sec. 4).

1. MODEL

In order to study the transitions from the ballistic regime of 2D electron transport to the hydrodynamic or the Ohmic ones, we consider a flow in a long sample with the width W and the length $L \gg W$ with the rough longitudinal edges (see Fig 1 in the main text). Herewith we use the simplified forms of the electron-electron and the disorder collision integrals, allowing the analytical solution of the kinetic equation. Such model has been developed in Refs. [28, 29] to study the ballistic transport of 2D interacting electrons in the limit of very low magnetic field, $B \rightarrow 0$ (here and below [1], [2], [3], and so are the references the main text).

We seek for the linear response of 2D electrons to a homogeneous electric field $\mathbf{E}_0 \parallel x$ in the presence of external magnetic field \mathbf{B} perpendicular to the sample plane (see Fig. 1 in the main text). The corresponding distribution function of 2D electrons acquires a nonequilibrium part:

$$\delta f(y, \mathbf{p}) = -f'_F(\varepsilon) f(y, \varphi, \varepsilon), \quad (\text{S1})$$

where $f_F(\varepsilon)$ is the Fermi distribution function, $\varepsilon = p^2/(2m)$ is the electron energy, φ is the angle between the electron velocity $\mathbf{v} = v(\varepsilon)[\sin \varphi, \cos \varphi]$ and the normal to the left sample edge (see Fig. 1 in the main text), $\mathbf{p} = m\mathbf{v}$ is the electron momentum, m is the electron mass, and the factor $f(y, \varphi, \varepsilon)$ is linear in E_0 : $f \sim E_0$. The dependence of δf on the coordinate x is absent since $L \gg W$. We also omit below the energy dependence of the electron velocity $v(\varepsilon) = \sqrt{2\varepsilon/m}$ and of the factor $f(y, \varphi, \varepsilon)$ in the nonequilibrium part of distribution function $\delta f(y, \mathbf{p})$. This simplification of f is valid for 2D degenerated electrons interacting by Coulomb's law for the viscous [30] and, apparently, the ballistic regimes of charge transport.

Hereinafter, we use the units in which the absolute value of the electron velocity, $v(\varepsilon) \equiv v_F$, and of the electron charge, e , are set to be unity. So coordinate, time, and reciprocal electric field, $1/E_0$, have the same units.

The kinetic equation for the nonequilibrium distribu-

tion function $f(y, \varphi)$ takes the form:

$$\cos \varphi \frac{\partial f}{\partial y} - \sin \varphi E_0 - \cos \varphi E_H - \omega_c \frac{\partial f}{\partial \varphi} = \text{St}[f], \quad (\text{S2})$$

where $\omega_c = eB/mc$ is the cyclotron frequency, E_H is the Hall electric field arising due to redistribution of electrons in the presence of magnetic field, and the collision integral $\text{St}[f]$ describes both momentum-conserving electron-electron collisions and dissipative scattering by bulk disorder:

$$\text{St}[f] = -\gamma f + \gamma_{ee} \hat{P}[f] + \gamma' \hat{P}_0[f], \quad (\text{S3})$$

where γ_{ee} and γ' are electron-electron and disorder scattering rates, $\gamma = \gamma_{ee} + \gamma'$ is the total scattering rate, \hat{P} and \hat{P}_0 are the projector operators of the functions $f(\varphi)$ onto the subspaces $\{1, e^{\pm i\varphi}\}$ and $\{1\}$, respectively. Such collision integral conserves perturbations of the distribution function corresponding to a nonequilibrium density. It also describes the conservation of momentum in the inter-particle scattering, when there is no disorder ($\gamma' = 0$).

We consider that the longitudinal sample edges are rough. Thus the scattering of electrons on them is diffusive and the boundary conditions for the distribution function take the form [29, 31]:

$$\begin{aligned} f(-W/2, \varphi) &= c_l, \quad -\pi/2 < \varphi < \pi/2, \\ f(W/2, \varphi) &= c_r, \quad \pi/2 < \varphi < 3\pi/2, \end{aligned} \quad (\text{S4})$$

(see also Fig. 1 in the main text). Here the quantities $c_l = c_l[f]$ and $c_r = c_r[f]$ are proportional to the y components of the incident particle flows on the left ($y = -W/2$) and the right ($y = W/2$) sample edges:

$$\begin{aligned} c_l &= -\frac{1}{2} \int_{\pi/2}^{3\pi/2} d\varphi' \cos \varphi' f(-W/2, \varphi'), \\ c_r &= \frac{1}{2} \int_{-\pi/2}^{\pi/2} d\varphi' \cos \varphi' f(W/2, \varphi'). \end{aligned} \quad (\text{S5})$$

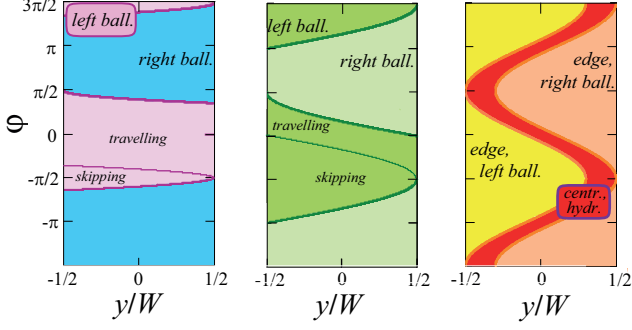


FIG. S1. Regions in the plane (y, φ) with the ballistic electrons, reflected from the left and the right sample edges (in all panels), as well as with the central hydrodynamic electrons, those do not scatter on the edges [red region in panel (c)]. The cases of narrow, $W \ll R_c$ (a); intermediate, $W \sim R_c$ (b); and wide, $W > 2R_c$ (c) samples are shown.

These boundary conditions indicate that (i) the probability of the electron reflection from the rough edges is independent on the reflection angle φ and (ii) the transverse component of the electron flow,

$$j_y(y) = \frac{n_0}{\pi m} \int_0^{2\pi} d\varphi' \cos \varphi' f(y, \varphi'), \quad (\text{S6})$$

vanishes at the edges, $j_y|_{y=\pm W/2} = 0$ [thus, it is zero everywhere in the sample, $j_y \equiv 0$, due to the continuity equation $\text{div } \mathbf{j} = j'_y = 0$].

The longitudinal current density along the sample is:

$$j(y) = \frac{n_0}{\pi m} \int_0^{2\pi} d\varphi' \sin \varphi' f(y, \varphi'). \quad (\text{S7})$$

If an electric current flows through a sample in a magnetic field, a perturbation of the charged density and the Hall electric field arise due to the magnetic Lorentz force. Both these effects are described by the zeroth ($m = 0$) angular harmonic of the distribution function:

$$f^{m=0}(y) = \frac{1}{2\pi} \int_0^{2\pi} d\varphi' f(y, \varphi'). \quad (\text{S8})$$

Figures S1(a,b) shows the regions in the (y, φ) -plane corresponding to the ballistic motion of electrons reflected from the right and from the left sample edges. Here and below in the current work we imply that the electron mean free path $l = 1/\gamma$ is much longer than the sample width. Therefore, most of electrons are not scattering in the bulk and move inside the left or the right regions by the ballistic trajectories between collisions with the edges.

For narrow samples, $W \ll R_c$, the left and the right ballistic regions are close to the rectangles $[-\pi/2, \pi/2] \times [-W/2, W/2]$ and $[\pi/2, 3\pi/2] \times$

$[-W/2, W/2]$ [see Fig. S1(a)]. For wider samples, $W \sim R_c$, $W < 2R_c$, the boundaries of the left and right region $\varphi_{\pm}(y)$ begin to significantly depend on coordinate y [see Fig. S1(b)]. The boundary curves $\varphi_+(y) = \arcsin[1 - \omega_c(W/2 + y)]$ and $\varphi_-(y) + \pi$, where $\varphi_-(y) = \arcsin[1 - \omega_c(W/2 - y)]$ coincide the electron trajectories those are touching the edges tangentially. Therefore the distribution function $f(y, \varphi)$ is not well defined at these curves. At magnetic fields above the critical field, $W > 2R_c$, the central electrons those do not scatter on the edges arise in the region filled with red in Fig. S1(c). Herewith the edge electrons in the left and right regions (yellow and pink) still scatter mainly on the edges.

It is useful to rewrite kinetic equation (S2) in the form:

$$\begin{aligned} & \left[\cos \varphi \frac{\partial}{\partial y} + \gamma \right] \tilde{f} - \sin \varphi E_0 = \\ & = \gamma_{ee} \hat{P}[\tilde{f}] + \gamma' \hat{P}_0[\tilde{f}] + \omega_c \frac{\partial \tilde{f}}{\partial \varphi}, \end{aligned} \quad (\text{S9})$$

where we have introduced the function:

$$\tilde{f}(y, \varphi) = f(y, \varphi) + \phi(y). \quad (\text{S10})$$

Here ϕ is the electrostatic potential of the Hall electric field: $E_H = -\phi'$. Indeed, it follows from Eq. (S2) that the Hall potential $\phi(y)$ plays the same role in the transport equation as its progenitor, the zero harmonic of the distribution function $f^{m=0}(y)$ (S8) being proportional to the inhomogeneous density perturbations. Therefore it is reasonable to introduce the function $\tilde{f}(y, \varphi)$ (S10) in order to take into account $\phi(y)$ and $f^{m=0}(y)$ within the same framework.

The zero harmonic $\tilde{f}^{m=0}(y)$ of the generalized distribution function (S10) takes the form:

$$\tilde{f}^{m=0}(y) = \delta\mu(y) + \phi(y), \quad (\text{S11})$$

where $\delta\mu$ is the perturbation of the electron chemical potential. In the case of sufficiently slow flows, the values $\delta\mu(y)$ and $\phi(y)$ are related by the electrostatic relations [21]. For the considered case of 2D degenerated electrons, ϕ is usually much greater than the related perturbation of the chemical potential $\delta\mu$ [21]. Thus the Hall electric field is calculated just by the formula $E_H(y) \approx -[\tilde{f}^{m=0}]'(y)$.

For brevity, we further omit the tilde in the function \tilde{f} and write $f \equiv \tilde{f}$.

2. BALLISTIC REGIME

2.1. Solution of kinetic equation in ballistic regime

In this section we consider the 2D electron transport in a long sample in relatively weak magnetic fields when the

diameter of the cyclotron circle is larger than the sample width, $2R_c > W$. Provided the bulk mean free path is much longer than the sample width, $l = 1/\gamma \gg W$, the dominant mechanism of scattering of most of electrons is collisions with the sample edges and the ballistic transport is realized.

In Ref. [28] the kinetic equation (S9) in the limits $\gamma W \gg 1$ and $\gamma W \ll 1$ at zero magnetic field was analyzed. It was demonstrated that in the first limit $\gamma W \gg 1$ the hydrodynamic regime is realized in the central region of the sample, $W/2 - |y| \gg 1/\gamma$. Herewith the departure and the arrival terms, $-\gamma_{ee}f$ and $\gamma_{ee}\hat{P}[f]$, are of the same order of magnitude, and Eq. (S9) is transformed into the Navier-Stokes equation for $j(y)$.

It was also shown in Ref. [28] that in the ballistic regime, $\gamma W \ll 1$, the arrival terms $\gamma_{ee}\hat{P}[f]$ and $\gamma'\hat{P}_0[f]$ in the right-hand side of Eq. (S9) are much smaller than the terms $\cos\varphi\partial f/\partial y$ and $\sin\varphi E_0$ in its left-hand side in the factor of $\gamma W \ln[1/(\gamma W)]$, therefore the first terms can be taken into account by the perturbation theory. Herewith the departure term γf in the left-hand side plays role of regularization of the kinetic equation near the angles $\varphi \approx \pm\pi/2$, where the cosine factor in the term $\cos\varphi\partial f/\partial y$ is close to zero.

In Ref. [29] the similar result for the arrival terms in Eq. (S9) at a nonzero magnetic field was obtained. Namely, in the weak magnetic fields, $\omega_c \ll \gamma^2 W$, the terms $\gamma_{ee}\hat{P}[f]$ and $\gamma'\hat{P}_0[f]$ should be treated as perturbations in the equations for the first-, $f_1 \sim \omega_c$, and the second-order, $f_2 \sim \omega_c^2$, corrections by magnetic field to the distribution function $f(y, \varphi)$ [the corrections $f_{1,2}$ are responsible for the Hall effect and the magnetoresistance].

Next, it is reasonable to expect that in narrow samples, $\gamma W \ll 1$, in the intermediate magnetic fields below the critical field:

$$\omega_c \sim 1/W, \quad \omega_c < 2/W, \quad (\text{S12})$$

the vanishing of the term $\cos\varphi\partial f/\partial y$ at $|\varphi| \approx \pi/2$ is ‘‘healed’’ by the magnetic field term $\omega_c\partial f/\partial\varphi$ and, thus, the electron flow at any φ is mainly determined by the scattering on the edges. The neglect of the collision terms in kinetic equation (S9) leads to the estimates:

$$f \sim E_0/\omega_c, \quad j \sim j_0, \quad E_H \sim E_0. \quad (\text{S13})$$

where $j_0 = n_0 E_0 W/m$. According to estimate (S13) of f , both the arrival and the departure terms in St are proportional to $(\gamma/\omega_c)E_0$, thus both they are much smaller than the other ballistic terms of Eq. (S9). In this way, the scattering of electrons in the bulk leads only to small corrections to the distribution function, proportional to $\gamma/\omega_c \ll 1$.

Below we will see that estimates (S13) are valid in the middle part of interval $0 < \omega_c W < 2$, which excludes the very weak fields, $0 < \omega_c W \ll 1$, as well as the lower vicinity of the critical point, $0 < 2 - \omega_c W \ll 1$. In the first

subinterval, the maximum length of the ballistic trajectories, determining j_0 and E_H , is achieved for the group of electrons moving almost along the sample [26, 28, 29]. In the second excluded subinterval, the ballistic size effects lead to the suppression of momentum relaxation in the scattering of electrons on the edges. As a consequence, the collisions of electrons in the bulk becomes more important than at $2 - \omega_c W \sim 1$ [we will show below that the role of the bulk scattering becomes comparable with the one of the purely ballistic scattering at $2 - \omega_c W \sim \gamma W$].

In this way, the ballistic regime is realized in the interval $0 < \omega_c W \lesssim 2$ (until $2 - \omega_c W \gg \gamma W$) and is divided on the three following subregimes. The first one is:

$$(i) \quad \omega_c \ll \gamma^2 W. \quad (\text{S14})$$

Magnetotransport in this subregime was partly studied in Refs. [28, 29]. The length $l_b^{(2)} = \sqrt{R_c W}$ of the maximal segment of a cyclotron circle inscribed in the stripe is longer than the bulk scattering length, $l_b^{(2)} \gg l = 1/\gamma$, therefore the longest ballistic trajectories are confined by l . The second subregime is:

$$(ii) \quad \gamma^2 W \ll \omega_c \ll 1/W \quad (\text{S15})$$

This case was partly studied in Refs. [25, 26]. The geometric parameter W/R_c is small as compared with unity and $l_b^{(2)} \ll 1/\gamma$, therefore the maximal trajectory length is limited by the purely ballistic dynamic and is equal to $l_b^{(2)}$. The bulk scattering provides small corrections to j and E_H . The third subregime is:

$$(iii) \quad \omega_c \sim 1/W, \quad 2 - \omega_c W \gg \gamma W \quad (\text{S16})$$

As far as we know, this subregime was not noticed and studied yet. In it, $W/R_c \sim 1$, thus the trajectory lengths are limited by W . The bulk scattering still provides only small corrections, but in the upper part of this interval, $\gamma W \ll 2 - \omega_c W \ll 1$, a peculiar geometry of trajectories leads to a suppression of the ballistic momentum relaxation (for details see Sec. 3.1). Effects of the last type are usually referred as the ballistic size effects.

According to the results of [25, 26, 28, 29] for the subregimes (i), (ii) and the above estimates characterizing the subregime (iii), in order to develop a unified description of the ballistic transport one should use kinetic equation (S9) with only the departure collision term retained:

$$\left[\cos\varphi \frac{\partial}{\partial y} + \gamma \right] f - \sin\varphi e E_0 = \omega_c \frac{\partial f}{\partial\varphi}. \quad (\text{S17})$$

This equation is solved by the method of characteristics for the first-order differential equations. Such solution was constructed in recent publication [26].

In our work, using a slightly different approach, we obtain the ballistic distribution function $f(y, \varphi)$ similar to the one obtained in Ref. [26]. We use this solution to study the regimes those were not considered in

Ref. [26]: the first ballistic subregime (i), $\omega_c W \ll \gamma^2 W^2$ (partly studied in Refs. [28],[29]) and the third ballistic subregime (iii), especially, its right singular part: $\gamma W \ll 2 - \omega_c W \ll 1$.

The solution of Eq. (S17) with boundary conditions (S4) and (S5) is a discontinuous function with the domains of continuity shown in Figs. S1(a,b). For the distribution function of the electrons reflected from the left edge, whose trajectories lie in the interval:

$$-\pi + \varphi_-(y) < \varphi < \varphi_+(y), \quad (\text{S18})$$

we use the notation: $f(y, \varphi) = f_+(y, \varphi)$ {in equation (S18) we introduced the values: $\varphi_{\pm}(y) = \arcsin[1 - \omega_c(W/2 \pm y)]$ }. For the electrons reflected from the right edge, whose trajectories are located in the interval:

$$\varphi_+(y) < \varphi < \pi + \varphi_-(y), \quad (\text{S19})$$

we use the analogous notation: $f(y, \varphi) = f_-(y, \varphi)$. The functions f_{\pm} are found by the standard, but lengthy calculations of the method of characteristics. We obtained:

$$f_{\pm}(y, \varphi) = \frac{E_0}{\gamma^2 + \omega_c^2} \left[\omega_c \cos \varphi + \gamma \sin \varphi + e^{\gamma\varphi/\omega_c} Z_{\pm}(\sin \varphi + \omega_c y) \right], \quad (\text{S20})$$

where the y -independent terms $\omega_c \cos \varphi$ and $\gamma \sin \varphi$ are particular solutions of Eq. (S17) those corresponds to the usual Drude formulas for a homogeneous Ohmic flow, whereas the term $e^{\gamma\varphi/\omega_c} Z_{\pm}(X)$ is a general solution of kinetic equation (S17) without the field term $\sin \varphi E_0$, allowing to satisfy the proper boundary conditions (S4).

By substituting Eq. (S20) into boundary conditions (S4), we obtain the explicit form of $Z_{\pm}(X)$:

$$Z_+(X) = e^{-\frac{\gamma}{\omega_c} \arcsin(X + \omega_c W/2)} \left[c_l - \gamma(X + \omega_c W/2) - \omega_c \sqrt{1 - (X + \omega_c W/2)^2} \right], \quad (\text{S21})$$

$$Z_-(X) = e^{-\frac{\gamma}{\omega_c} [\pi - \arcsin(X - \omega_c W/2)]} \left[c_r - \gamma(X - \omega_c W/2) + \omega_c \sqrt{1 - (X - \omega_c W/2)^2} \right]. \quad (\text{S22})$$

The coefficients c_l and c_r in these formulas are determined from balance relations (S5) of the boundary conditions. The resulting linear equations for c_l and c_r takes the form:

$$\begin{pmatrix} I_{ll} & I_{lr} \\ I_{rl} & I_{rr} \end{pmatrix} \begin{pmatrix} c_l \\ c_r \end{pmatrix} = - \begin{pmatrix} I_l \\ I_r \end{pmatrix}, \quad (\text{S23})$$

where the coefficients in the first line of the matrix are expressed via the integrals:

$$I_{ll} = 2 + \int_{-\pi + \varphi_0}^{-\pi/2} d\varphi \cos \varphi e^{\frac{\gamma}{\omega_c} (\pi + 2\varphi)}, \quad (\text{S24})$$

$$I_{lr} = \int_{\pi/2}^{\pi + \varphi_0} d\varphi \cos \varphi e^{\frac{\gamma}{\omega_c} [\varphi - \pi + \arcsin(\sin \varphi - \omega_c W)]}, \quad (\text{S25})$$

while the first components of the right-hand vector is:

$$I_l = \frac{\pi \omega_c}{2} + \int_{\varphi_0}^{\pi/2} d\varphi \cos \varphi \times e^{\frac{\gamma}{\omega_c} (2\varphi - \pi)} (\omega_c \cos \varphi - \gamma \sin \varphi) - \int_{-\pi/2}^{\varphi_0} d\varphi \cos \varphi e^{\frac{\gamma}{\omega_c} [\varphi - \arcsin(\sin \varphi + \omega_c W)]} \times [\omega_c \sqrt{1 - (\sin \varphi + \omega_c W)^2} + \gamma (\sin \varphi + \omega_c W)]. \quad (\text{S26})$$

The other coefficients in Eq. (S23), I_{rr} , I_{rl} and I_r , are related to I_{ll} , I_{lr} , and I_l by the formulas: $I_{rr} = -I_{ll}$, $I_{rl} = -I_{lr}$, $I_r = I_l$. In Eqs. (S24)-(S26) we introduced the notation: $\varphi_0 = \arcsin(1 - \omega_c W)$.

At general values of the parameter $\omega_c W$, integrals (S24)-(S26) can be calculated only numerically. However, the explicit expressions for these integrals and the resulting values $c_{l,r}$, $j(y)$, and $E_H(y)$ can be obtained in the limiting cases: $\omega_c W \ll (\gamma W)^2$ [the first ballistic subregion (i)]; $(\gamma W)^2 \ll \omega_c W \ll 1$ [the second ballistic subregion (ii)]; and $\gamma W \ll 2 - \omega_c W \ll 1$ [the right singular part of the third ballistic subregion (iii)].

2.2. Ballistic transport in moderate magnetic fields

The estimates from Sec. 2.1 show that in the interval of magnetic fields $(\gamma W)^2 \ll \omega_c W \lesssim 1$ provided that $2 - \omega_c W \gg \gamma W$ [the second and the third ballistic subregimes] the electron flow in the main order by γ is determined by taking into account only the action of the external fields and the scattering on the rough sample edges. The interparticle scattering provides only small corrections to all values, proportional to $\gamma W \ll 1$.

In this way, the asymptote of Eq. (S20) by $\gamma \rightarrow 0$ provides the distribution function describing the flow in the main order by γW :

$$f_{\pm}(y, \varphi) = \tilde{c}_{l,r} + \frac{E_0}{\omega_c} \left\{ \cos \varphi \mp \sqrt{1 - \left[\sin \varphi + \omega_c \left(y \pm \frac{W}{2} \right) \right]^2} \right\}, \quad (\text{S27})$$

where $\tilde{c}_{l,r} = E_0 c_{l,r} / \omega_c^2$. Linear system (S17) is degenerate at $\gamma = 0$, thus its solution $\tilde{c}_{l,r}$ can be determined up to a constant c_0 . Note that at $\gamma > 0$ function (S20), with $\tilde{c}_{l,r}$ calculated from non-degenerate system (S17), implies a weak artefact relaxation of the electron density due to the neglect in Eq. (S17) of the arrival terms $\gamma_{ee} P[f]$ and

$\gamma'P_0[f]$. Imposing the symmetric condition $c_l + c_r = 0$ corresponding to $c_0 = 0$, from Eq. (S23) we obtain:

$$\tilde{c}_{l,r} = \mp \frac{E_0}{\omega_c} \frac{U - V}{2(2 - \omega_c W)}, \quad (\text{S28})$$

where $U = \arccos(1 - \omega_c W)$, and $V = (1 - \omega_c W)\sqrt{\omega_c W(2 - \omega_c W)}$. Solution (S27)-(S28) was recently obtained in Ref. [26].

A description of the profiles of the current $j(y)$ and the Hall field $E_H(y)$ corresponding to Eq. (S27) as well as a detailed justification of the applicability of Eq. (S27) in the moderately weak magnetic fields, $(\gamma W)^2 \ll \omega_c W \lesssim 1$, will be published in another publication. In this work we present only the simplest properties of the purely ballistic flow.

In the limit $\omega_c W \ll 1$ distribution (S27) at the angles $\sqrt{\omega_c(W/2 \pm y)} \ll |\varphi| - \pi/2 \ll 1$ takes the form:

$$f_{\pm}(y, \varphi) = \tilde{c}_{l,r} + E_0 \left[y_{\pm} \frac{\sin \varphi}{\cos \varphi} + \frac{\omega_c y_{\pm}^2}{2 \cos^3 \varphi} \right]. \quad (\text{S29})$$

where and $y_{\pm} = y \pm W/2$ and $\tilde{c}_{l,r} = \pm E_0 \sqrt{3\omega_c W^3}/2$. From Eqs. (S27) and (S29) we obtain for the current density $j(y)$ in the whole interval of the moderate magnetic fields $(\gamma W)^2 \ll \omega_c W \lesssim 1$ [provided $2 - \omega_c W \gtrsim 1$, that is until the vicinity of B_c]:

$$j \sim j_0 \ln(1/\sqrt{\omega_c W}), \quad (\text{S30})$$

where $\sqrt{\omega_c W} = W/l_b^{(2)}$ is the maximum angle between the sample direction x and the longest ballistic trajectories at $y = \pm W/2$ (see Fig. 1 in the main text). Equation (S30) expresses the fact that the main contribution to j comes from such trajectories with the lengths $\sim l_b^{(2)}$. At $\omega_c W \sim 1$ estimate (S30) coincides with Eq. (S13).

In the whole interval $(\gamma W)^2 \ll \omega_c W \lesssim 1$ [provided $2 - \omega_c W \gtrsim 1$] distributions (S27) and (S29) leads to the above estimate (S13) for the Hall field: $E_H \sim E_0$.

In the lower vicinity the transition point, $\gamma W \ll 2 - \omega_c W \ll 1$ [the right part of the third ballistic subregime], the coefficients $\tilde{c}_{l,r}$ diverge as $1/(2 - \omega_c W)$, thus the main part of the distribution function is :

$$f_{\pm}(y, \varphi) = \pm \frac{\pi E_0}{2 \omega_c (2 - \omega_c W)}. \quad (\text{S31})$$

The other terms of Eq. (S27) have the smaller order of magnitude: $\sim E_0/\omega_c$. Function f_{\pm} (S31) describes the imbalance between the densities of the electrons reflected from the left and the right edges, a part of which, the ‘‘travelling electrons’’ those reach the opposite edges, compensates the $\mathbf{E}_0 \times \mathbf{B}$ -drift contribution in $j_y = 0$ [the term $E_0 \cos \varphi/\omega_c$ in Eq. (S27)].

The current j and the Hall field E_H corresponding to f_{\pm} with (S31) also diverge as $1/(2 - \omega_c W)$ at the near-transition region $\gamma W \ll 2 - \omega_c W \ll 1$. The exact formulas for them will be presented below in Sec. 3 with taking into account also a weak scattering in the bulk.

2.3. Ballistic transport in very weak magnetic fields

In the first ballistic subregime, $\omega_c \ll \gamma^2 W$, the continuity domains of $f_{\pm}(y, \varphi)$ given by Eqs. (S18) and (S19) become close to $-\pi/2 < \varphi < \pi/2$ and $\pi/2 < \varphi < 3\pi/2$ at any y [see Fig. S1(a)]. Most of electrons are the ‘‘travelling’’ ones whose trajectories of are slightly bent lines starting on one edge and ending on another.

In Refs. [28, 29] a solution of Eq. (S17) in the limit $\omega_c \rightarrow 0$ based on the perturbation theory by the magnetic field term $\partial f/\partial \omega_c$ was constructed. Up to the second order in ω_c , such solution has the form:

$$f = f_0 + f_1 + f_2, \quad (\text{S32})$$

where f_0 is the distribution function in zero magnetic field, while $f_1 \sim \omega_c$ and $f_2 \sim \omega_c^2$.

In this subsection, first, we refine the applicability of the perturbation approach of Refs. [28, 29]. Comparison of the magnetic field term, $\omega_c \partial f/\partial \varphi$, in the kinetic equation with the other terms, $\cos \varphi \partial f/\partial y$ and $-\gamma f$, at the angles $|\varphi| \rightarrow \pi/2$ shows that the effect from a magnetic field can be treated as a perturbation for the travelling electrons in the central bulk part of the sample:

$$W/2 - |y| \gg \omega_c/\gamma^2. \quad (\text{S33})$$

At such y , power decomposition (S32) for the distribution function is valid, which leads to the results obtained in [28, 29] for the contributions of region (S33) to the transport characteristics of the sample.

However, in the very vicinities of the sample edges,

$$W/2 - |y| \lesssim \omega_c/\gamma^2, \quad (\text{S34})$$

the magnetic field term $\omega_c \partial f/\partial \varphi$ cannot be treated as a perturbation for few ‘‘skipping’’ electrons with $|\varphi| \approx \pi/2$, which are returning to the same edge after the scattering on it (see Fig. 1 in the main text). Their flow is almost collisionless, being similar to the one studied in Sec. 2.2. Criteria (S33) and (S34) follow from the comparison of the two possible limitations of the ballistic trajectories lengths at $|\varphi| \rightarrow \pi/2$: the size $\sqrt{R_c(W/2 - |y|)}$ of the cyclotron circle segment with the height $(W/2 - |y|)$ or the bulk scattering length, $l = 1/\gamma$.

In Refs. [28, 29] the possibility of the formation of the near-edge regions where the perturbation theory by ω_c becomes not applicable was missed.

In realistic samples, the near-edges regions can be formed only in not too small magnetic field in the samples with long and straight edges. Namely, the near-edge layer width ω_c/γ^2 must be larger than the size of edges roughnesses. At the very vicinity of $B = 0$, $\omega_c < \omega_c^* \ll \gamma^2 W$, the flow in the near-edge layers becomes controlled by a particular shape of roughnesses. At such ω_c , the bulk contributions to the current and the Hall field, described in [28, 29], may dominate and determine the sample resistances ρ_{xx} and ρ_{xy} .

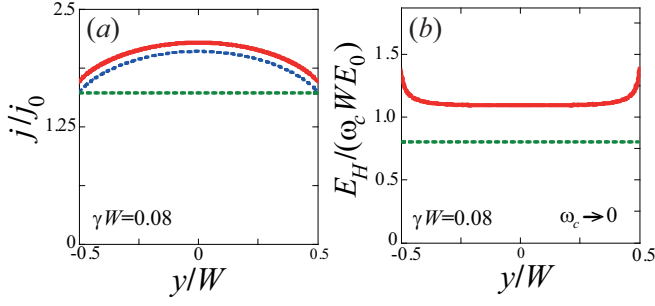


FIG. S2. Current density (a) and Hall field (b) in the bulk part of a sample, $W/2 - |y| \gg \omega_c/\gamma^2$, at $\gamma W = 0.08$ and in the limit $\omega_c \rightarrow 0$ [the left part of the first ballistic sub-regime]. Red curves present numerical results obtained from Eqs. (S35), (S38), and (S39). Blue curve in panel (a) correspond to analytical solution (S36), while green curve shows the main contribution to the current density $j = j_\gamma$. Green curve in panel (b) is plotted according to Eq. (S41).

Second, in this subsection we derive the asymptote of the function f_\pm (S20) at $\omega_c \ll \gamma^2 W$ by the small parameter $\omega_c/(\gamma^2 W)$ and the resulting contributions to $j(y)$ and $E_H(y)$. Such asymptote corresponds to the travelling electrons and provides the main part of f_\pm in the bulk region (S33) at any φ [thus the main contributions in j and E_H there] as well as the values of f_\pm in the near-edge regions (S34) at the velocity angles $|\pi/2 - |\varphi|| \gg \sqrt{\omega_c(W/2 - |y|)}$. The same asymptotic form of f_\pm , j , and E_H in the bulk region were obtained in Refs. [28, 29] within the perturbation approach: a direct solution of the kinetic equation in the limits $\gamma W \ll 1$ and $\omega_c \ll \gamma^2 W$.

In the zeroth order by ω_c , functions f_\pm (S20) take the well-known form [28],[31]:

$$f_{0,\pm}(y, \varphi) = E_0 \frac{\sin \varphi}{\gamma} \left[1 - \exp\left(-\gamma \frac{y \pm W/2}{\cos \varphi}\right) \right], \quad (\text{S35})$$

with the zero coefficients $c_{l,r}$. The flow density corresponding to Eq. (S35) in the leading order by the parameter γW is homogeneous, while an y -dependence emerges in the next order by γW [28]:

$$\begin{aligned} j(y) &= j_\gamma + \Delta j(y), \\ \frac{j_\gamma}{j_0} &= \frac{2}{\pi} \ln\left(\frac{1}{\gamma W}\right), \quad j_0 = \frac{n_0 E_0 W}{m}, \\ \frac{\Delta j(y)}{j_0} &= -\frac{2}{\pi} \left[\left(\frac{1}{2} + \frac{y}{W}\right) \ln\left(\frac{1}{2} + \frac{y}{W}\right) + \right. \\ &\quad \left. + \left(\frac{1}{2} - \frac{y}{W}\right) \ln\left(\frac{1}{2} - \frac{y}{W}\right) \right]. \end{aligned} \quad (\text{S36})$$

The contribution $\Delta j(y)$ has infinite derivatives at the sample edges $y = \pm W/2$ [see Fig. S2(a)].

The logarithmic divergence of j_γ in Eq. (S35) by γW originates from the travelling electrons with the veloc-

ity angles in the diapason: $||\varphi| - \pi/2| \lesssim \delta_m^\pm(y)$, where $\delta_m^\pm(y) = \gamma(W/2 \pm y) \ll 1$. Such electrons move almost parallel to the sample and spend much longer time between scattering at the edges, acquiring much larger contribution to their velocities v_x due to acceleration by E_0 , as compared with other electrons with the angles $\varphi \sim 1$.

Direct calculations yield that the first order term in the expansion of f_\pm (S20) coincides with the function f_1 obtained in Ref. [29] in a perturbation solution of Eq. (S17). Such f_1 satisfies the nontrivial boundary conditions (S4) with $c_{l,r} \neq 0$ and can be written as:

$$f_1 = f_1^z + f_1^b, \quad (\text{S37})$$

where the first term

$$\begin{aligned} f_{1,\pm}^z(y, \varphi) &= \omega_c E_0 \left\{ \frac{\cos \varphi}{\gamma^2} - \exp\left[-\gamma \frac{y \pm W/2}{\cos \varphi}\right] \right. \\ &\quad \left. \times \left[\frac{\cos \varphi}{\gamma^2} + \frac{y \pm W/2}{\gamma} - \frac{\sin^2 \varphi}{2 \cos^3 \varphi} \left(y \pm \frac{W}{2}\right)^2 \right] \right\} \end{aligned} \quad (\text{S38})$$

is the solution of the inhomogeneous kinetic equation ($E_0 \neq 0$) with zero boundary conditions, while the term

$$f_{1,\pm}^b(y, \varphi) = \mp \omega_c E_0 \frac{W}{4\gamma} \exp\left(-\gamma \frac{y \pm W/2}{\cos \varphi}\right), \quad (\text{S39})$$

being the solution of the kinetic equation with $E_0 = 0$, ensures that boundary conditions (S4) are met. The function $f_{1,\pm}^b$ is much smaller than $f_{1,\pm}^z$ at $||\varphi| - \pi/2| \lesssim \delta_m^\pm(y)$, however $f_{1,\pm}^b$ and $f_{1,\pm}^z$ give comparable contributions to j_y in boundary condition (S4) require that $j_y(y = \pm W/2) = 0$.

Combining of Eqs. (S38), (S39), and (S8), we obtain for the zero harmonic of f_1 :

$$f^{m=0}(y) = -E_0 \frac{\omega_c y W}{\pi} \ln[1/(\gamma W)]. \quad (\text{S40})$$

for the Hall field in the central bulk region (S33) in the leading order by γW [29]:

$$E_H(y) = E_0 \frac{\omega_c W}{\pi} \ln\left(\frac{1}{\gamma W}\right). \quad (\text{S41})$$

The numerically calculated exact profile $E_H(y)$ corresponding to Eqs. (S38) and (S39) differs from this analytical formula (S41) on the values of the order of $E_0 \omega_c W$ [see Fig. S2(b)]. It is noteworthy that the perturbation theory result (S41) is linear by magnetic field, like it takes place for the Hall field in bulk conductors.

Formulas (S36) and (S41) lead to the following expression for the local Hall resistance $\varrho_{xy}(y) = E_H(y)/j(y)$:

$$\varrho_{xy} \approx \frac{1}{2} \varrho_{xy}^{(0)}, \quad \varrho_{xy}^{(0)} = \frac{m \omega_c}{n_0} = \frac{B}{n_0 e c}, \quad (\text{S42})$$

where $\varrho_{xy}^{(0)}$ is the conventional Hall resistance for the Ohmic and the hydrodynamic flows of charged particles at low temperatures [17].

The second-order correction $f_2 \sim \omega_c^2$ to the electron distribution function was calculated in Ref. [28]. At the velocity directions being close to the sample direction, $|\varphi| - \pi/2 \ll 1$, the function f_2 in the central region (S33) in the main order by $1/(\gamma W)$ has the form:

$$f_2(y, \varphi) = \frac{\omega_c^2 E_0 (y \pm W/2)^3}{2 \cos^5 \varphi} \times \left[1 - \frac{\gamma (y \pm W/2)}{4 \cos \varphi} \right] \exp \left[- \frac{\gamma (y \pm W/2)}{\cos \varphi} \right]. \quad (\text{S43})$$

This correction leads to the following magnetic-field dependence of the current density in region (S33):

$$j(y) \approx j_\gamma + j_2, \quad j_2 = \frac{3n_0 E_0}{2\pi m} \frac{\omega_c^2}{W\gamma^4}. \quad (\text{S44})$$

The origin of correction (S45) consists in a small increase of the mean length of the trajectories of the travelling electrons due to the action of the weak magnetic field (see discussion and Fig. 1 in Ref. [28]).

The positive correction j_2 (S44) to the current j_γ leads to a small negative magnetoresistance of the bulk region:

$$\frac{\varrho_{xx}(B) - \varrho_{xx}(0)}{\varrho_{xx}(0)} = - \frac{3\omega_c^2}{4\gamma^4 W^2 \ln[1/(\gamma W)]}, \quad (\text{S45})$$

where $\varrho_{xx} = E_0/j(y)$. It was discussed in Refs. [28, 29] that for not too long samples, $W \ll L \ll 1/\gamma$, the bulk scattering rate γ in this formula is replaced on the reciprocal sample length, $1/L$, and magnetoresistance (S45) becomes temperature-independent. Moreover, it was discussed that result (S45) is applicable even for the narrow short samples with the lengths $L \sim W \ll 1/\gamma$. In the last case, the rate γ should be replaced just on $1/W$:

$$\frac{\varrho_{xx}(B) - \varrho_{xx}(0)}{\varrho_{xx}(0)} \sim -\omega_c^2 W^2. \quad (\text{S46})$$

In such short samples, only the ballistic subregimes $\omega_c W \ll 1$ and $1 \lesssim \omega_c W \lesssim 2$, analogous the first and the third subregimes for the long samples, are realized, so result (S46) is valid until $\omega_c \ll 1/W$.

Third, we study the flow in the near-edge regions (S34).

It can be seen from Eq. (S20) that for y in (S34) one of the components of the distribution function f_\pm (S20) [namely, f_+ at $y \approx -W/2$ and f_- at $y \approx W/2$] takes the form of the purely ballistic function f_\pm (S27) of the second subregime with the coefficients $\tilde{c}_{l,r}$ corresponding the low-B-limit function $f_{1,\pm}^b$ (S39):

$$\tilde{c}_{l,r} = \mp \omega_c E_0 W / (4\gamma). \quad (\text{S47})$$

Such components f_\pm at the angles φ near to the sample direction:

$$|\pi/2 - |\varphi|| \lesssim \delta_\pm(y), \quad \delta_\pm(y) = \sqrt{\omega_c(W/2 \pm y)}, \quad (\text{S48})$$

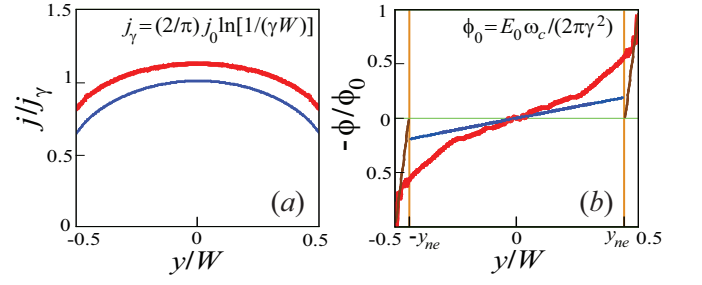


FIG. S3. Current density $j(y)$ [a] and the potential $\phi_H(y) = -\phi'_H(y)$ [b] at a finite magnetic field in the first ballistic subregime, $\omega_c \ll \gamma^2 W$, in the whole sample, $|y| < W/2$. The vertical dashed lines depict the boundaries $\pm y_{ne}$, $y_{ne} = W/2 - \omega_c/\gamma^2$ of the near-edge regions (S34). The parameters of the flow are: $\omega_c W = 0.01$, $\gamma W = 0.3$. Red curves on both panels present numerical results obtained by general formula (S20). Blue curves on both panels present the results of the perturbation theory for the bulk region, Eqs. (S36) and (S41). Brown curves on panel (b) show the non-perturbation result (S49) for the near edge-regions.

has finite values $\sim E_0 \sqrt{W/\omega_c}$, while at the angles $\delta_\pm(y) \ll |\pi/2 - |\varphi|| \ll 1$ are close to asymptotic formula (S29). The last one is equal to Eqs. (S35) and (S37) in the main order by $\gamma W \ll 1$ [note that $\delta_\pm(y) \gg \delta_m^\pm(y) = \gamma(W/2 \pm y)$ in the near-edge layers]. The other components of the distribution function, f_+ at $y \approx W/2$ and f_- at $y \approx -W/2$, are still described by Eqs. (S35) and (S37) with the characteristic angles $\delta_m^\pm(y)$, separating the regions of large and small magnitudes of f_\pm .

Analysis of electron trajectories shows that such distribution functions f_\pm (S20) in the layers, $y \approx \mp W/2$, at the angles $|\pi/2 - |\varphi|| \lesssim \delta_\pm(y)$ describe the purely ballistic skipping electrons.

The zero harmonic $f^{m=0}$ of the described distribution f_\pm in the near-edge regions $y \approx \pm W/2$ (S34) takes the form:

$$f^{m=0}(y) \approx \mp \frac{E_0 \omega_c}{2\pi} \left[\frac{1}{\gamma^2} - C \frac{W/2 \mp y}{\omega_c} \right], \quad (\text{S49})$$

where $C \sim 1$ is a numeric coefficient. Such $f^{m=0}$ is much larger than its value in the bulk region, Eq. (S40). Both the terms in expression $f^{m=0}(y)$ (S49) originate the biggest singular terms $\sim 1/\cos^3 \varphi$ in the f_+ and f_- components given by Eqs. (S38) and (S29). For y in bulk region (S33), such part in $f^{m=0}(y)$ corresponding to the $\sim 1/\cos^3 \varphi$ -terms in f_\pm vanishes, as for the bulk function $f_{1,\pm}^z$ (S38) the contributions in $f^{m=0}(y)$ of this order from $f_{1,+}$ and $f_{1,-}$ compensate each other.

So the anomalous behavior of $f^{m=0}(y)$ in the near-edges layers [compare (S40) and (S49)] is related with the decomposition of the divergent contributions ($\sim 1/\gamma^2$) in $f^{m=0}(y)$ from the travelling electrons reflected from one edge in the vicinities of the opposite edge due to the appearance of the skipping electrons.

Equation (S49) leads to the Hall field in near-edge regions (S34), similar to one in the subregime (ii) in the whole sample:

$$E_H(y) \sim E_0, \quad W/2 - |y| \lesssim \omega_c/\gamma^2. \quad (\text{S50})$$

In this way, the field $E_H(y)$ is strongly enhanced in the near-edge regions and becomes non-analytical by ω_c [see Eqs. (S41), (S50) and Fig. S3(b)]. The resulting Hall voltage $U_H = \phi(W/2) - \phi(-W/2)$ takes the form:

$$U_H = -E_0 \omega_c / (\pi \gamma^2), \quad (\text{S51})$$

that correspond to an anomalously large Hall resistance $\varrho_{xy} = U_H/(Wj)$:

$$\varrho_{xy} = \varrho_{xy}^{(0)} / \{2\gamma^2 W^2 \ln[1/(\gamma W)]\}. \quad (\text{S52})$$

From a similar analysis of the $m = 1$ angular harmonic of general distribution f_{\pm} (S20) in near-edge regions $y \approx \mp W/2$ (S34), we obtain for the current density in the main order by $\delta_m^{\pm}(y) \sim \gamma W$ and $\delta_{\pm}(y) \sim \sqrt{\omega_c W}$:

$$j(y) \approx \frac{2j_0}{\pi} \left\{ \left(\frac{1}{2} \pm \frac{y}{W} \right) \ln \left[\frac{1}{\sqrt{\omega_c(W/2 \pm y)}} \right] + \left(\frac{1}{2} \mp \frac{y}{W} \right) \ln \left[\frac{1}{\gamma(W/2 \mp y)} \right] \right\}. \quad (\text{S53})$$

The logarithms in both the first and the second term are estimated as $\ln(\gamma/\omega_c)$ at typical y in layers (S34). For the deviation of the averaged current density, $j = \int_{-W/2}^{W/2} j(y) dy/W$, from its value in zero magnetic field:

$$\begin{aligned} \delta j_e &= j - j_{\gamma} - \frac{1}{W} \int_{-W/2}^{W/2} dy \Delta j(y) \sim \\ &\sim j_0 \int_0^{\Delta\xi} d\xi \xi \left[\ln \left(\frac{1}{\sqrt{\omega_c W \xi}} \right) - \ln \left(\frac{1}{\gamma W \xi} \right) \right], \end{aligned} \quad (\text{S54})$$

we obtain from Eqs. (S36) and (S53):

$$\delta j_e \sim -j_0 \frac{\omega_c^2}{\gamma^4 W^2} \ln \left(\frac{\gamma}{\omega_c} \right). \quad (\text{S55})$$

In Eq. (S54) we introduced the values $\xi = 1/2 - |y|/W$ and $\Delta\xi = \omega_c/(\gamma^2 W)$. Derived correction δj_e (S55) leads to a positive nonanalytical by ω_c magnetoresistance:

$$\frac{\varrho_{xx}(B) - \varrho_{xx}(0)}{\varrho_{xx}(0)} \sim \frac{\omega_c^2 \ln(\gamma/\omega_c)}{\gamma^4 W^2 \ln[1/(\gamma W)]}, \quad (\text{S56})$$

Such magnetoresistance accounts the non-perturbative in B effect of the skipping electrons on the flow in the near-edge regions. Namely, the marginal angles $\delta_m^{\pm}(y)$ of the travelling electrons, which determines the main contribution to $j(y)$ and $E_H(y)$ in the bulk region, are changed in the near-edge regions on the purely ballistic angles

$\delta_{\pm}(y)$ (S48), $\delta_{\pm}(y) \gg \delta_m^{\pm}(y)$, separating the trajectories of the skipping and the travelling electrons.

In realistic samples, depending on their geometry both the bulk or the edge contributions to magnetoresistance and the Hall effect may appear. For long samples of very high quality, where the described above skipping trajectories are realized near the longitudinal edges, the resistances ϱ_{xx} and ϱ_{xy} will be determined by near-edge regions (S34), as contributions (S52), (S56) from those regions to the magnetic field-dependent parts of j and E_H are greater than from bulk contributions (S41), (S45). For samples with a more irregular geometry (not very long and straight), the contribution from the near-edge regions is to be suppressed, thus bulk magnetoresistance (S45) and bulk Hall effect (S42) may be observed.

We also note that the particular experimental setup, in particular, the exact positions y_i of the electrical contacts will determine the manifestation of the bulk or of the near-edge contributions to ϱ_{xx} and ϱ_{xy} even in long high-quality stripes.

Fourth, we present in this subsection an elementary ‘‘kinematic’’ derivation of equations (S41) and (S42), being one of the main result of Ref. [29]. Such derivation elucidates why the local ballistic Hall resistance at $\omega_c \rightarrow 0$ in the bulk of a sample is equal to one half of the conventional Hall resistance of Ohmic samples, $\varrho_{xy}^0 = B/(n_0 e c)$.

Formulas (S36), (S41), and (S44) for the integral characteristics of the flow in the bulk region (S33) were derived from kinetic equation (S17) with the departure term $-\gamma f$ and the magnetic field term $\omega_c \partial f / \partial \varphi$. According to the above consideration, this implies that all electrons accounted in this calculation are the travelling ones. After the scattering at edges, they reach the opposite edges without inter-particle collisions (at $|\varphi - \pi/2| \gg \gamma W$) or undergo an inter-particle collision in the bulk (at $|\varphi - \pi/2| \lesssim \gamma W$). Herewith the main contributions to current (S36) and Hall field (S41) comes from the electrons with the angles $\gamma W \lesssim |\pi/2 - \varphi| \ll 1$.

Let us consider the kinematics of such travelling electrons. In the limit $\omega_c \rightarrow 0$ and $E_0 \rightarrow 0$, their trajectories $\mathbf{r}(t) = [x(t), y(t)]$ are almost straight lines. For the x component of the velocity $\mathbf{v} = \dot{\mathbf{r}}$ of an electron reflected by the angle φ from the left edge we have:

$$v_x(t, \varphi) = v_F \sin \varphi + (eE_0/m) t, \quad (\text{S57})$$

where the time t is counted from the moment of the reflection. In Eqs. (S57) and until the end of this subsection we again explicitly write v_F and e for a better comprehension of the text.

According to the definition of the mean current density j (the mean amount of charge passing through the sample section per unit time), its value in the ballistic regime is calculated by an analog of the Drude formula:

$$j = n_0 e^2 t_0 E_0 / m, \quad (\text{S58})$$

where t_0 is the mean time of a free motion of electrons. Such t_0 for the travelling electrons is calculated by the averaging over all proper φ of the times $t_{\pm}(y = \pm W/2, \varphi)$ of collisionless motion of the electrons with initial velocity angles φ . Here the value $t_{\pm}(y, \varphi)$ denotes the time of motion of an electron by the zero-field trajectory ($E_0, B = 0$) with the initial angle φ starting at $y_0 = \mp W/2$, and ending in the point y , $-W/2 < y < W/2$:

$$t_{\pm}(y, \varphi) = \frac{W/2 \pm y}{v_F |\cos \varphi|}. \quad (\text{S59})$$

To find t_0 , one needs to integrate $t_{\pm}(y = \pm W/2, \varphi)$ by φ up to the limiting values of $\varphi_m^{\pm} \approx \pm\pi/2$ at which $|\pi/2 - |\varphi||$ is equal to $\delta_m^{\pm}(y = \pm W/2) = \gamma W$. Such limits correspond to the ballistic trajectories with the maximum length equal to the mean free path relative to the bulk scattering, $l = 1/\gamma$. After the integration, we obtain $j \approx j_{\gamma}$ in the main order by γW , where $j_{\gamma} = (2/\pi)j_0 \ln[1/(\gamma W)]$ is defined in Eq. (S36).

Next, we calculate the Hall field E_H in bulk region (S33) within a similar approach. We suppose E_H to be homogeneous in that region: $E_H(y) \approx E_H$. We find E_H from the y component of Newton's equations:

$$m\dot{v}_y = eE_H - (eB/c)v_x. \quad (\text{S60})$$

After the averaging of this equation at any y over the travelling electrons with various φ , only the contribution $\Delta v_x(t) = (eE_0/m)t$ in v_x related to the acceleration by the field E_0 [see Eq. (S57)] remains non-zero. There is no acceleration along the y direction of the ensemble of the travelling electrons in the bulk region:

$$\sum_{\pm} \int_{-y_{ne}}^{y_{ne}} \frac{dy}{W} \Re \int_0^{2\pi} \frac{d\varphi}{2\pi} m\dot{v}_y[t_{\pm}(y, \varphi), \varphi] = 0, \quad (\text{S61})$$

where $y_{ne} = W/2 - \omega_c/\gamma^2$ is the boundary of the right near-edge region and the symbol \Re denotes the exclusion the vicinities of the angles $\pm\pi/2$ of the size γW in the integral by $d\varphi$. This exclusion corresponds to the neglect of the electrons scattered in the bulk on other electrons. From equality (S61) and equation (S60) averaged over all travelling electrons in the bulk region by the same way as in (S61) we obtain:

$$E_H = \frac{B}{c} \sum_{\pm} \int_{-y_{ne}}^{y_{ne}} \frac{dy}{W} \Re \int_0^{2\pi} \frac{d\varphi}{2\pi} v_x[t_{\pm}(y, \varphi), \varphi]. \quad (\text{S62})$$

In the limit $E_0, B \rightarrow 0$ this equation, together with equation Eqs. (S58) and (S59), yields in the main order by γW : $E_H = (1/2)(B/c)j_{\gamma}/(en_0)$, which is result (S41).

In view of the above elementary consideration, it becomes apparent that the factor 1/2 in Eqs. (S41) and (S42) has a kinematic origin. Indeed, the above value of E_H follows from condition (S62) of the compensation of the linearly increasing in time magnetic Lorenz force,

$(eB/c)\Delta v_x(t)$, by the Hall field force eE_H . The resulting E_H contains the mean time of motion t_0 of the travelling electrons between the edges and the factor 1/2 due to integrating of $\Delta v_x(t_{\pm}(y, \varphi))$ over y [see Eqs. (S57), (S59), and (S62)]. Expression (S58) for j contains the same time t_0 with no numeric factors. Thus the local ballistic Hall resistance $\varrho_{xy} = E_H(y)/j(y)$ acquires the additional factor 1/2 as compared with ϱ_{xy} in the Ohmic and the hydrodynamic regimes. We remind that in the last regimes for the flows of the same geometry ($j_y \equiv 0$), the value E_H is calculated from the balance of the mean forces eE_H and $(eB/c)j/(en_0)$ acting on fluid elements with given macroscopic values $j = j_x(y)$.

3. BALLISTIC-HYDRODYNAMIC AND BALLISTIC-OHMIC PHASE TRANSITIONS

3.1. Semiballistic solution near critical field

The model formulated in Sec. 1 allows one to consider the systems being the mixtures of the two cases: (i) there are no bulk defects and the electrons inside the sample are scattered only on each other, conserving momentum; and (ii) there are no inter-particle collisions, but inside the sample the scattering of electrons on a weak disorder, leading to a weak momentum relaxation, takes place. For simplicity, we consider only these unmixed types of samples with only one of the scattering mechanisms: the electron-electron collisions ($\gamma = \gamma_{ee}, \gamma' = 0$) or the scattering on disorder ($\gamma = \gamma', \gamma_{ee} = 0$). Herewith we always consider that the scattering rates are weak:

$$\gamma W \ll 1, \quad (\text{S63})$$

that is the main condition of applicability of our theory.

In this subsection, we analyze ballistic solution (S20) in the whole lower vicinity $0 < 2 - \omega_c W \ll 1$ of the critical point, including the region $2 - \omega_c W \sim \gamma W$. This distribution function takes into account the departure term, $-\gamma f$, in the collision operator. Thus it provides an exact description of the flow at $\omega_c W < 2$ in the disordered samples with no electron-electron scattering (that is, of the lower vicinity of the ballistic-Ohmic phase transition). In next subsections, we will also use function (S20) in the region $0 < 2 - \omega_c W \lesssim \gamma W$ for pure samples with only the interparticle scattering as a trial solution to construct the mean-field model of the lower vicinity of the ballistic-hydrodynamic phase transition.

The $\mathbf{E} \times \mathbf{B}$ -drift flow $j_y^{(0)}$ in the y direction, described by the space-homogeneous Drude part of the distribution function (S20), is compensated only by the travelling electrons reaching the opposite edge, as the skipping electrons, provide no contribution in j_y due to the symmetry of their trajectories (see Fig. 1 in the main text).

The coefficients I_{ll}, I_{lr} of the system of linear equations (S23) tend to zero at $2 - \omega_c W \ll 1$. From Eqs. (S24) and

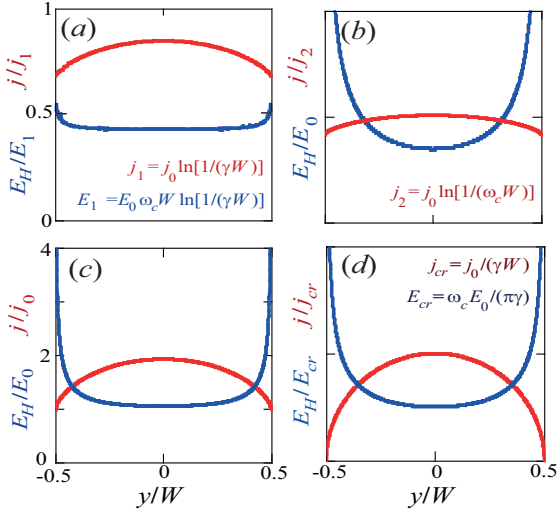


FIG. S4. Profiles of the current density (red curves) and the Hall electric field (blue curves) at different values of magnetic field: (a) the first ballistic subregime in the limit $\omega_c \rightarrow 0$ for the ballistic parameter $\gamma W = 0.08$ (only the bulk of the sample is shown); (b) the second ballistic subregime, corresponding to the small parameter $\omega_c W$, $\omega_c W = 10^{-3}$ [herewith $\omega_c W \gg (\gamma W)^2$]; (c) the third ballistic subregime at the intermediate parameter $\omega_c W$, $\omega_c W = 1$; and (d) the very point of the phase transition, when $\omega_c W = 2$ [within approximation (S75) of the proposed mean field model]. Curves are plotted by Eqs. (S7) and (S8) with distribution function (S35), (S38), (S39) for (a); with function (S27) for (b) and (c); by formulas (S67), (S75), and (S70) for (d).

(S25) for I_{ll} and I_{lr} in main order by the small parameters $2 - \omega_c W \ll 1$ and $\gamma/\omega_c \ll 1$ we have:

$$I_{ll} = 2 - \omega_c W + 2\pi\gamma/\omega_c, \quad I_{lr} = 2 - \omega_c W. \quad (\text{S64})$$

Herewith, it follows from Eq. (S26) that the right-hand side coefficients in Eq. (S23) remains finite at $B \rightarrow B_c$: $I_l = -\pi\omega$. Equations (S23) with the above values $I_{ll,lr,l}$ yield for the parameters c_{\pm} in distribution function (S20):

$$c_{\pm} = \pm \omega_c^2 / (2\gamma + u\omega_c), \quad (\text{S65})$$

where the small parameter $u = u(B) \sim B_c - B$,

$$u = (2/\pi)(2 - \omega_c W), \quad 0 < u \ll 1, \quad (\text{S66})$$

originates from I_{ll} , I_{lr} and characterizes the proximity to the transition point at the fields below the critical point $\omega_c^{cr} = 2/W$. It is proportional to the small relative density, $\alpha_{tr} \sim u$, of the travelling electrons those compensate the $\mathbf{E}_0 \times \mathbf{B}$ -drift contribution in j_y . Coefficients c_{\pm} (S65) have a divergent behavior at $\omega_c \rightarrow \omega_c^{cr}$, becoming much larger than $c_{\pm}|_{\omega_c W \sim 1}$, whereas other terms in general solution f_{\pm} (S20) have no divergence at $\omega_c \rightarrow \omega_c^{cr}$. Thus the distribution function (S20) in the man order by the small parameters $2 - \omega_c W$ and γW is given by:

$$f_{\pm}(y, \varphi) = \pm \frac{E_0}{2\gamma + u\omega_c}. \quad (\text{S67})$$

Such f_{\pm} is a generalization of purely ballistic solution (S31) and additionally accounts the electron scattering in the bulk. This scattering provides much larger corrections in f_{\pm} (of the relative order of $\gamma W/u$) in the upper part of the third ballistic regime, $\gamma W \ll u \ll 1$, than in the intermediate fields, when $u \sim 1$. The effects from the scatterings in the bulk and on the edges become comparable at $u \sim \gamma W$ [see Eq. (S67)].

Expressions f_{\pm} (S67) describe a redistribution of the skipping and the travelling electrons between the left and the right regions (S18) and (S19). The redistribution of the travelling electrons contribute in j_y , compensating the $\mathbf{E} \times \mathbf{B}$ -drift. The redistribution of the skipping electrons provides no contribution in j_y due to the symmetry of their trajectories. As $\alpha_{tr} \sim u$ and $c_{\pm} \sim 1/u$, the full density of the travelling electrons, $\sim \alpha_{tr} c_{\pm}$, corresponds by the order of magnitude to the $\mathbf{E} \times \mathbf{B}$ -drift terms in general solution (S20). The appearance of the skipping electrons with the relative density $\alpha_{sk} \sim 1$ and divergent full density, $\alpha_{sk} c_{\pm} \sim 1/u$, originate from the equal probabilities of the scattering on the edges for all angles φ .

Beside this, there is also a small group of electrons, with the proportion $\alpha_{\gamma} \sim \gamma W$, which would have returned to the same edge or reach the other one, but due to the scattering in the bulk have changed their trajectories. Such electrons leads to an additional compensation of the $\mathbf{E} \times \mathbf{B}$ -drift and, thus, weakens the imbalance between the left and the right skipping electrons. So the divergence of c_{\pm} (S65) at $u \rightarrow 0$ is limited by the rate γ .

The current density and the Hall field for function (S67) in the main orders by γ and u takes the forms:

$$j(y) = \frac{4nE_0}{\pi m} \frac{1}{2\gamma + u\omega_c} \sqrt{1 - \omega_c^2 y^2}, \quad (\text{S68})$$

$$E_H(y) = \frac{2E_0}{\pi} \frac{1}{2\gamma + u\omega_c} \frac{\omega_c}{\sqrt{1 - \omega_c^2 y^2}}. \quad (\text{S69})$$

These profiles as well as $j(y)$ and $E_H(y)$ in the three ballistic subregimes are plotted in Fig. S4. For the averaged current density $j = \int_{-W/2}^{W/2} dy j(y)/W$ and Hall field $E_H = \int_{-W/2}^{W/2} dy E_H(y)/W$ we obtain:

$$j = \frac{n_0 E_0 / m}{2\gamma + u\omega_c}, \quad E_H = \frac{E_0 \omega_c}{2\gamma + u\omega_c}. \quad (\text{S70})$$

It is of importance to perform a more precise calculation of the current density j and the Hall electric field E_H for the critical distribution function (S67). In the next order by the small parameter \sqrt{u} we obtain the same equation (S70) for j , but the corrected result for E_H :

$$E_H = \frac{E_0 \omega_c}{2\gamma + u\omega_c} F(u), \quad F(u) = 1 - \sqrt{\frac{2}{\pi} u}. \quad (\text{S71})$$

The factor $F(u)$ describes the correction from the deviation of the shapes of the left and the right ballistic regions from their limiting form at $u = 0$.

For brevity, below we omit the factor n_0/m in all current densities. That is, we change the units of the current densities according to: $j \rightarrow j/[n_0/m]$.

The obtained values of j and E_H (S70) at the very critical point, $u = 0$, turn out to be one half as compared with the Dude results for j and E_H of a bulk sample with the same width, the rate $\gamma' = \gamma$ of the scattering on disorder, and no interparticle collisions. This fact implies that, for such disordered samples, the diffusive scattering on the edges and the scattering on the bulk disorder at $W = 2R_c$ provide the comparable contributions to the total momentum relaxation rate, 2γ .

3.2. Mean field theory below critical field

In this section we develop a model of the “near-transitional” flow in pure samples with interacting electrons in the nearest lower vicinity of the critical field,

$$0 < 2 - \omega_c W \lesssim \gamma W. \quad (\text{S72})$$

At such ω_c , the substitution of distribution function f_{\pm} (S67) into the departure and the arrival terms, γf and $\gamma \hat{P}[f]$, leads to the values of the same order of magnitude, $\sim E_0$, as the other terms in kinetic equation (S9). This indicates that both the terms γf and $\gamma \hat{P}[f]$ are equally important in the near-transition interval (S72).

Instead of the exact solution of Eq. (S9), we propose a mean-field approach of the description of the electron dynamics in interval (S72) based on an approximate accounting for the arrival term $\gamma \hat{P}[f]$. Namely, we treat the part of this term:

$$\gamma \hat{P}_{\sin}[f](y, \varphi) = \gamma j(y) \sin \varphi, \quad (\text{S73})$$

as the appearance of the addition “internal” field $\Delta E_0(y) \sim \gamma j(y)$ in the truncated kinetic equation (S17). Herewith we will omit the dependence of $j(y)$ on the coordinate y , replacing in $\Delta E_0 \sin \varphi$ (S73) the current density $j(y)$ by its average value $j = \int_{-W/2}^{W/2} dy j(y)/W$.

The substitution of the function f_{\pm} (S67) into the arrival term $\gamma \hat{P}[f]$ leads also to the term $\gamma f^{m=0}(y)$ and the term $\gamma \cos \varphi j_y(y)$ with a small non-physical current $j_y(y) \sim u$, appearing due to the non-exact form of solution (S67). Such terms with $j_y(y)$ and $f^{m=0}(y)$ also can be interpreted within the mean-field approach as the other internal fields in the truncated kinetic equation of the type of (S17). However, our analysis shows that these terms induce the contributions in f_{\pm} , j , and E_H which are relatively small by the parameters γW and u in interval (S72), as compared with the effect from the sin-term (S73) with j corresponding to f_{\pm} (S67).

It was shown in Refs. [28, 29] that, for the first ballistic subregime, $\omega_c \ll \gamma^2/W$, the similar approach of the solution of Eq. (S9) based on the independent on y approximation of $\gamma \hat{P}[f]$ is asymptotically exact by the parameter

$\ln[1/(\gamma W)] \gg 1$ [see Eq. (S36)]. Near the transition, the ballistic current density $j(y)$ (S68) is strongly inhomogeneous, thus such approach should lead to an inaccurate calculation of numerical coefficients in all values. However, in view of the success of similar mean-field methods for thermodynamic phase transitions, one can expect that this approach will provide a qualitatively correct results. Comparison in next section of our final results with the preceding numerical theory and experiments also testifies to the good applicability of our method.

The replacement of the term $\gamma \hat{P}[f]$ by its value average by y can be interpreted as using of a special, nonlocal by y , collision integral:

$$\text{St}'[f] = -\gamma \left\{ f(y, \varphi) - \int_{-W/2}^{W/2} \frac{d\tilde{y}}{W} \hat{P}[f](\tilde{y}, \varphi) \right\}. \quad (\text{S74})$$

Such operator conserves momentum and number of electrons only within the whole sample, but not at any y .

In this way, the mean field equation for the averaged current $j = j(u)$, which determines the state of the system, is constructed by the substitution:

$$E_0 \rightarrow \tilde{E}_0 = E_0 + \gamma j \quad (\text{S75})$$

in the ballistic equation (S70) for j . After such substitution, we obtain the self-consistent equation for j in the ballistic-hydrodynamic region (S72):

$$j = \frac{E_0 + \gamma j}{2\gamma + u\omega_c}. \quad (\text{S76})$$

Solution of this equation is:

$$j = \frac{E_0}{\gamma + u\omega_c}. \quad (\text{S77})$$

In the very transition point, $u = 0$, this value is twice as large compared with the fully ballistic result (S70), neglecting the arrival term $\gamma \hat{P}[f]$.

It was discussed in Sec. 3.1 that semiballistic function (S67) describe a shortage of the skipping electrons near one of the edge and the excess near the other one (as compared with the equilibrium state). The mean-field current (S77) additionally accounts for the conserving of momentum in interparticle collisions. The magnitudes of (S67) and (S77) correspond to the compensation of the $\mathbf{E} \times \mathbf{B}$ -drift along the y direction [the first term in Eq. (S20)]. This compensation is realized due to: (i) motion of the few travelling electrons along the trajectories connecting opposite edges and (ii) the interparticle scattering of both the skipping and the travelling electrons in the bulk. These two processes correspond to the two terms, $\sim u\omega_c$ and $\sim \gamma$, in the denominators of Eqs. (S67), (S70), and (S77).

In disordered samples, each scattering of an electron on a defect leads to the loss of its inequilibrium momentum and to a shift of the center of its trajectory. In

pure samples, each collision of two electrons induces only shifts of the centers of their trajectories. As a result, the scattering on the bulk disorder is twice more effective for momentum relaxation than the electron-electron scattering with the same rate $\gamma = \gamma'$ within our mean-field approach [compare Eqs. (S70) and (S77)].

The Hall electric field in the lowest vicinity (S72) of the ballistic-hydrodynamic transition is calculated by the replacement $E_0 \rightarrow E_0 + \gamma j$ in semiballistic result (S71) for the Hall field:

$$E_H = (E_0 + \gamma j) \frac{\omega_c}{2\gamma + u/W} F(u). \quad (\text{S78})$$

We emphasize that this equation, unlike Eqs. (S75) and (S76), does not participate in the self-consistent procedure of determining the state of the system. Substituting the mean field current j (S77) in Eq. (S78) we obtain:

$$E_H = E_0 \frac{\omega_c}{\gamma + u\omega_c} F(u). \quad (\text{S79})$$

Due to the factor $F(u)$, this function, like as $E_H(u)$ (S71), has a strong square-root singularity at $\omega_c W \rightarrow 2$.

The above results for the third ballistic subregime $\gamma W \ll 2 - \omega_c W \lesssim 1$ and for the nearest vicinity of B_c (S72) are apparently valid also for not too long, $W \ll L \ll l$, and even for short samples, $W \sim L \ll l$. Indeed, the size of all the electron trajectories in the x direction at $1 \lesssim \omega_c W < 2$ is confined by the cyclotron diameter. Thus the distribution function in these regimes is formed in the regions of the stripe of the lengths $\Delta L \sim W \approx 2/\omega$. It follows from this circumstance that one can independently consider segments with the lengths ΔL and account their contribution to the total resistance of a long sample by summation, like as for subsequently connected resistors.

3.3. Mean field theory above critical field

When the diameter of the cyclotron circle becomes smaller than the sample width, $W > 2R_c$, there arises a group of the ‘‘central electrons’’ whose trajectories do not cross the sample edges [see Fig. S1(c) and Fig. 1(c) in the main text]. Such electrons spend a long time, $\sim 1/\gamma \gg W$ on their trajectories without collisions. We will show in this Section that they form a pre-fluid collectivized fraction inside the dominant part of the semiballistic ‘‘edge electrons’’ those are scattered at the edges. The central electrons are crucial for both the ballistic-hydrodynamic and the ballistic-Ohmic phase transitions, occurring in pure and in disordered samples, respectively.

Below we formulate the two-component mean field model based on kinetic equation (S9) to describe the dynamics of the central and the edge electrons in the upper vicinities of these two phase transitions:

$$0 < \omega_c W - 2 \ll 1. \quad (\text{S80})$$

This model is a direct extension of the one-component mean field model formulated in Sec. 3.2. The relative density of the central electrons,

$$\alpha_c = (W - 2R_c)/W \sim B - B_c, \quad \alpha_c \ll 1, \quad (\text{S81})$$

is the order parameter of these transitions at the fields above the critical point: $0 < B - B_c \ll B_c$. The proportion of the edge electrons $\alpha_e = 1 - \alpha_c$ is close to unity.

The distribution functions f_e and f_c of the edge electrons (‘‘e’’) and of the central electrons (‘‘c’’) are defined in the two distinct regions in the (y, φ) plane [see Fig. S1(c)]. To describe the whole flow, one should solve the exact kinetic equation (S9) in such regions with accounting of both the arrival and the departure terms.

In order to find the distribution f_c of the central electrons, it is convenient to change the variables y, φ on the new variables y_c, φ , where y_c is the coordinate of the center of electron cyclotron orbits. The new variables of the central electron lie in the interval:

$$-W/2 + R_c < y_c < W/2 - R_c, \quad 0 < \varphi < 2\pi. \quad (\text{S82})$$

For the coordinates of the centers of the edge electrons trajectories we have:

$$|y_c| > W/2 - R_c, \quad (\text{S83})$$

while their velocity angle φ lies in the diapasons depending on y_c . However, we do not need to describe in detail the distribution f_e of the edge electrons, as their dynamics is similar to the one of the skipping electrons in the nearest low vicinity of the transition (S72) and therefore below we will apply for them the results of Sec. 3.2.

The solution $f_{c,e}(y_c, \varphi)$ of the exact kinetic equation (S9) with the non-local arrival term $\gamma \hat{P}[f_e + f_c]$ (or $\gamma \hat{P}_0[f_e + f_c]$) is a continuous function in diapason (S82). Therefore the angular harmonics $f_{c,m} \sim \int d\varphi f_c(y_c, \varphi) e^{-im\varphi}$ of f_c rapidly decrease with the increase of m (apparently, as a geometric progression). On the contrary, the studied above ballistic solutions f_{\pm} (S20), (S67) of Eq. (S17), describing also the edge electrons, has discontinuities at the marginal trajectories shown in Figs. S1. Thus functions f_{\pm} (S67) has angular harmonic depending on m slowly, as a power of m . In this way, the central electrons has the distribution function of a hydrodynamic type, being substantially different from ballistic function f_{\pm} (S67), therefore they constitute a nucleus of the viscous or the Ohmic flow.

Instead of an exact solution of kinetic equation (S9), we propose, following to Sec. 3.2, a two-component mean field model which accounts for the interparticle scattering with the neglect of the inhomogeneity of the arrival term $\gamma \hat{P}[f_e + f_c]$ by y . This model is to be qualitatively applicable in the nearest upper vicinity of the phase transition (S80), where the relative part of the central electrons is small, $\alpha_c \ll 1$. The exact form of such model is different for the pure and the disordered samples.

First, we study the ballistic-hydrodynamic transition in pure samples when only the electron-electron scattering takes place.

When the fraction of the central electrons is small, $\alpha_c \ll 1$, the centers y_c of their cyclotron orbits lie approximately in the center of the sample, $y = 0$ [see Eq. (S82) and Fig. 1(c) in the main text]. Herewith central electrons most often scatter on the edge electrons, which have the distribution $f_e(y_c, \varphi)$ varying by y_c on the scale of the order W . Thus the properties of all central electrons in the main orders by γ and α_c are almost identical and are described by the function f_c weakly depending on y :

$$f_c(y_c, \varphi) \approx f_c(0, \varphi). \quad (\text{S84})$$

Within our mean-field approach, we use the only one parameter to describe the state of the central electrons. It is their contribution, $j_c \sim f_c$, to the averaged current density j . Correspondingly, for the description of the state of the edge electrons we also use the similar mean field parameter, j_e , being the second contribution to the averaged current j .

To find j_e , we note that at $\alpha_c \ll 1$ kinetic equation (S9) with the arrival term simplified according to Eqs. (S74) and (S75) are applicable also for the edge electrons in their regions on the (y, φ) -plane [see Fig. S1(c)]. Thus in the main order by $\gamma W \ll 1$ the distribution f_e of these electrons at $\alpha_c \ll 1$ is the function f_{\pm} (S67) with $u = 0$, the proper shifts of the variable y , and the substitutions:

$$E_0 \rightarrow \tilde{E}_0 = E_0 + \gamma(j_e + j_c), \quad (\text{S85})$$

and $W \rightarrow \tilde{W} = 2R_c$. The last change accounts for the decrease with B of the total width \tilde{W} of the regions containing the edge electrons. The integration of such function f_e with the factor $\sin \varphi$ over the left and the right semiballistic edge regions of the width \tilde{W} (see Fig. S1) yields the formula for the edge electron contribution j_e to full current j , which contains \tilde{E} (S85) and is similar to Eq. (S76) obtained from the integration of f_{\pm} (S67) with \tilde{E} (S75) over the whole sample. In the main order by α_c and γW we obtain:

$$j_e = \alpha_e \frac{E_0 + \gamma(j_e + j_c)}{2\gamma}, \quad (\text{S86})$$

where the factor α_e takes into account the relative edge electron density [compare Eqs. (S86) and (S76)].

In order to calculate j_c , we multiply the kinetic equation (S9) expressed in the variables φ, y_c on the factor $\sin \varphi$ and integrate it by φ and y_c over $-\pi/2 < \varphi < 3\pi/2$ and $-W/2 + R_c < y_c < W/2 - R_c$. In this diapason of y_c , the distribution function f_c describes the central electrons and is approximately independent on y_c , according to Eq. (S84). As the result, we arrive to the formula:

$$j_c = \alpha_c \frac{E_0 + \gamma(j_e + j_c)}{\gamma}. \quad (\text{S87})$$

This is actually the Drude formula for the contribution to the total current from central electrons, which are scattered on the edge electrons with the rate γ and accelerated by the effective field (S85).

Solving together the resulting mean-field system of equations (S86) and (S87), keeping in mind that $\alpha_e + \alpha_c = 1$, we obtain in the zero and first orders by α_c :

$$j_e = \frac{E_0}{\gamma}, \quad j_c = 2\alpha_c \frac{E_0}{\gamma}. \quad (\text{S88})$$

For the total current $j = j_e + j_c$ we obtain from Eq. (S88):

$$j = (1 + 2\alpha_c) \frac{E_0}{\gamma}. \quad (\text{S89})$$

According to Eq. (S81) for α_c , this function grows linearly with the difference $B - B_c$.

The physical picture implied under the second equation in formulas (S88) is as follows. The dynamics of the central electrons in the reference frame moving with the effective drift velocity of the edge electrons [$v_{d,e} = 1/\gamma$, see Eq. (S88)] is similar to the scattering on static defects. Namely, the edge electrons as a whole are looked like static defects for the central electrons in this moving frame. The effective momentum relaxation time of the edge electrons due scattering on the edges and on other electrons is $1/\gamma$ [see the first equation in formula (S88)]. The scattering time of the central electrons on the edge electrons is also $1/\gamma$. As the drift velocity of the central electrons $v_{d,c}$ is the sum of and their drift velocity in the moving frame $v'_{d,c} = 1/\gamma$ and the velocity of the frame $v_{d,e}$, a doubling of the scattering time $1/\gamma$ in the equation for j_c in Eqs. (S88) arises.

The Hall field above the transition also contains the contributions from the edge electrons and from the central ones. As the ballistic solution f_{\pm} (S67) at $u = 0$ with the effective field \tilde{E}_0 and the change $W \rightarrow 2/\omega_c$ provides the distribution f_e of the edge electrons in interval (S80), the edge electrons contribution to the Hall field is given by the semiballistic value E_H (S71) with $u = 0$ and the changes $E_0 \rightarrow \tilde{E}_0$ (S85) and $W = 2/\omega_c^{cr} \rightarrow 2/\omega_c$. Herewith we should use Eq. (S89) for the current j in \tilde{E}_0 (S85) and add the factor α_e accounting for the relative density of the edge electrons. We obtain:

$$E_{H,e} = \alpha_e (1 + \alpha_c) \frac{\omega_c}{\gamma} E_0, \quad (\text{S90})$$

where we should put: $\alpha_e (1 + \alpha_c) = 1 - \alpha_c^2 \approx 1$.

The contribution to the Hall field from the central electrons is calculated using the y -independent distribution function f_c (S84). Multiplying kinetic equation (S9) on $\cos \varphi$ and integrating over $-\pi/2 < \varphi < 3\pi/2$ and $-W/2 + R_c < y_c < W/2 - R_c$, we obtain the contribution to the Hall field, similar to the Drude model result:

$$E_{H,c} = \omega_c j_c. \quad (\text{S91})$$

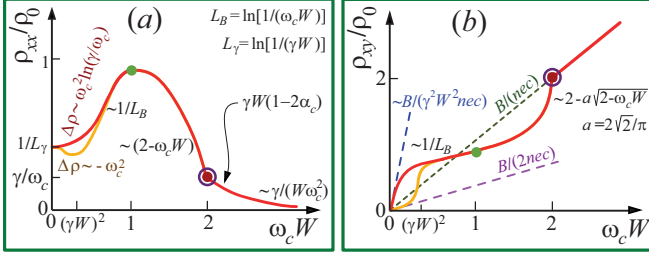


FIG. S5. Longitudinal ρ_{xx} (a) and Hall ρ_{xy} (b) resistances (schematically) as functions of magnetic field for a defectless sample normalized on the nominal ballistic resistance $\rho_0 = m/(ne^2W)$. In the first ballistic region ($R_c \gg l^2/W$) the resistances of the whole sample with straight edges, including the near-edge regions, (red curves) as well as of the bulk part of the sample without accounting the near-edge regions (orange curves) are drawn.

Substituting Eq. (S88) for j_c in this formula, we get for the total averaged Hall field $E_H = E_{H,e} + E_{H,c}$:

$$E_H = (1 + 2\alpha_c) \frac{\omega_c}{\gamma} E_0. \quad (\text{S92})$$

For the longitudinal $\rho_{xx} = E_0/j$ and the Hall $\rho_{xy} = E_H/j$ resistances we obtain from Eqs. (S77), (S79), (S89), and (S92) in the both vicinities of the ballistic-hydrodynamic phase transition, $|\omega_c W - 2| \ll 1$:

$$\rho_{xx}(B) = \frac{m\gamma}{n_0 e^2} \begin{cases} 1 + 2u/(\gamma W), & B < B_c \\ 1 - 2\alpha_c, & B > B_c \end{cases} \quad (\text{S93})$$

and

$$\rho_{xy}(B) = \frac{B}{n_0 e c} \begin{cases} 1 - \sqrt{u/\pi}, & B < B_c \\ 1, & B > B_c \end{cases}. \quad (\text{S94})$$

In these resulting formulas we again use the usual units for clarity. We remind that $u(B) = (2/\pi)(2 - \omega_c W) \sim B_c - B$ and $\alpha_c(B) = 1 - \omega_c W/2 \sim B - B_c$. It is noteworthy that the Hall resistance ρ_{xy} above the transition, $B > B_c$, coincides with its value in the Ohmic regime at zero temperature, $\rho_{xy}^{(0)} = B/(n_0 e c)$, at least, in the main order by γW in which all our calculations are performed.

In Fig. S5 we schematically draw the longitudinal and the Hall resistances $\rho_{xx}(B)$ and $\rho_{xy}(B)$ in the whole considered diapason of B : the three ballistic subregimes as well as the upper and lower vicinities of the ballistic-hydrodynamic transition,

Second, let us consider the ballistic-Ohmic phase transition in a sample in which the scattering only on disorder in the bulk is substantial. For clarity, below we will use the explicit notation γ' for the rate of the electron scattering on disorder.

In such system, the contribution to the current from the edge and from the central electrons are independent. For the contributions to j and E_H from edge electrons

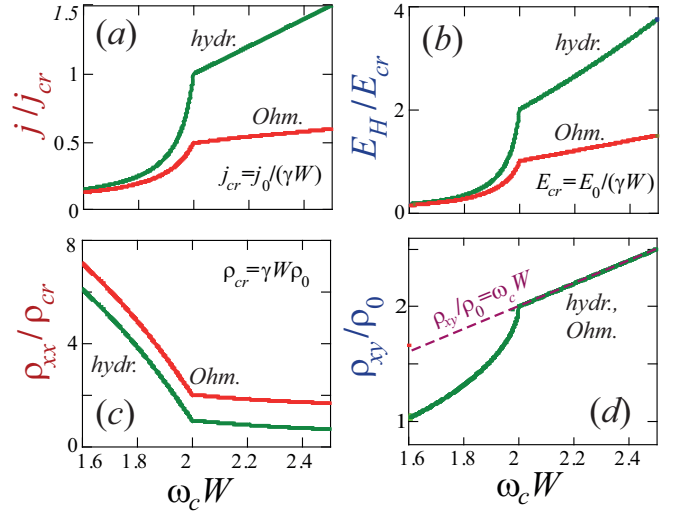


FIG. S6. Current (a), Hall electric field (b), longitudinal (c) and Hall (d) resistances as functions of magnetic field in a wide region around the critical field, $\omega_c^{cr} = 2/W$, for the ballistic-hydrodynamic phase transition [green curves] and for the ballistic-Ohmic phase transition [red curves]. In panel (d) for the Hall resistances, the green and the red curves referring to these to transitions coincide. All curves are plotted for the same values of the interparticle and the disorder scattering rates: $\gamma = \gamma'$.

one should use the pure ballistic formulas (S70) at $u = 0$, multiplied on the fraction of the edge electrons α_e :

$$j_e = \alpha_e \frac{E_0}{2\gamma'}, \quad E_{H,e} = \alpha_e \frac{\omega_c}{2\gamma'} E_0. \quad (\text{S95})$$

For the contribution to the current and the Hall field from the central electrons we should use the Drude formulas with the “bare” field E_0 and the factor α_c accounting their relative density:

$$j_c = \alpha_c \frac{E_0}{\gamma'}, \quad E_{H,c} = \alpha_c \frac{\omega_c E_0}{\gamma'}. \quad (\text{S96})$$

Keeping in mind that $\alpha_c + \alpha_e = 1$, for the total averaged current density and the averaged Hall field we obtain:

$$j = \frac{1 + \alpha_c}{2} \frac{E_0}{\gamma'}, \quad E_H = \frac{1 + \alpha_c}{2} \frac{\omega_c E_0}{\gamma'}. \quad (\text{S97})$$

Unlike the pure samples where only the electron-electron scattering takes place in the bulk, results (S97) remains valid in the disordered samples at any relation between the fractions α_c and α_e of electrons of the both groups. In particular, in the limit of very magnetic large fields, when $W \gg R_c$ and $\alpha_c \approx 1$, equations (S97) turn into the usual Drude formulas for long Ohmic samples.

Equations (S70), (S71), and (S97) lead to the following result for the longitudinal resistance in the both vicinities of the ballistic-Ohmic transition, $|\omega_c W - 2| \ll 1$:

$$\rho_{xx}(B) = \frac{2m\gamma'}{n_0 e^2} \begin{cases} 1 + u/(\gamma'W), & B < B_c \\ 1 - \alpha_c, & B > B_c \end{cases}, \quad (\text{S98})$$

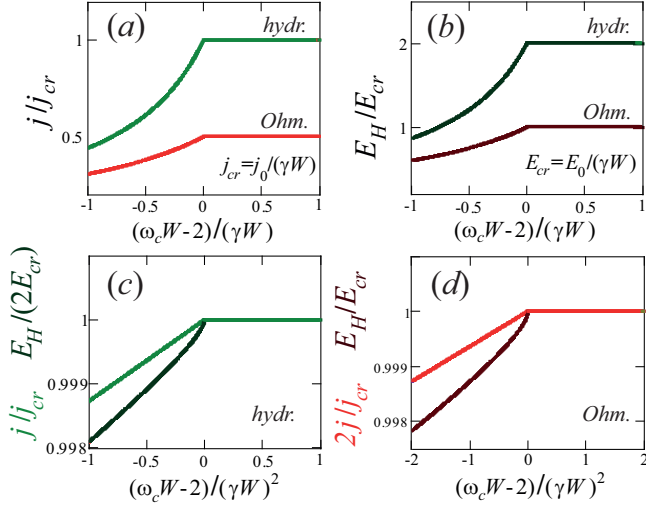


FIG. S7. Current and Hall electric field as functions of magnetic field in narrow (a,b) and very narrow (c,d) vicinities of the critical point $\omega_c^{cr} = 2/W$ for the ballistic-hydrodynamic and for the ballistic-Ohmic phase transition. All curves are plotted for the same values of the interparticle and the disorder scattering rates: $\gamma = \gamma'$.

while to the Hall resistance identical with result (S94) for the ballistic-hydrodynamic transition.

In Fig. S6 and Fig. S7 we draw the values j and E_H in the fields above and below the critical point $\omega_c^{cr} = 2/W$ [Eqs. (S77), (S79), (S89), (S92), and Eqs. (S97)], together with the corresponding resistances ϱ_{xx} and ϱ_{xy} [Eqs. (S93), (S94), and (S98)], for both the ballistic-hydrodynamic and the ballistic-Ohmic transitions in wide and narrow vicinities the critical magnetic field $\omega_c^{cr} = 2/W$. We see from Figs. S5-S7 that, in both the ballistic-hydrodynamic and the ballistic-Ohmic phase transitions, the current $j(\omega_c)$ and the longitudinal resistance $\varrho_{xx}(\omega_c)$ have a jump of its derivative (a kink) at the critical field $\omega_c^{cr} = 2/W$, while the Hall field $E_H(\omega_c)$ and resistance $\varrho_{xy}(\omega_c)$ have even a square-root singularity at $\omega_c \rightarrow \omega_c^{cr} - 0$ (see Figs. S6 and S7).

Third, we briefly discuss the behavior of the hydrodynamic and Ohmic flows far beyond the transition, when $W - 2R_c \sim W$ and $W - 2R_c \approx W \gg R_c$. In this cases, the fraction of the central electrons is comparable or greater than the one of the edge electrons: $\alpha_c \sim \alpha_e \sim 1$ or $\alpha_c \approx 1$, $\alpha_e \ll 1$. The collisions between the central electrons becomes important. The central electrons located farther from the edges are less likely to collide with edge electrons than central electrons located closer to the edge. Such character of the scattering leads to the formation of an inhomogeneous, parabolic by y , profile $j(y) \sim [(W/2)^2 - y^2]$ of the Poiseuille flow.

The region $W/R_c - 2 \gtrsim 1$ of the mixed hydrodynamic-ballistic and the Ohmic-ballistic flows were studied by the numeric solution of the kinetic equation in Refs. [25, 26]. For the ballistic-Ohmic transition, formulas (S97) for j

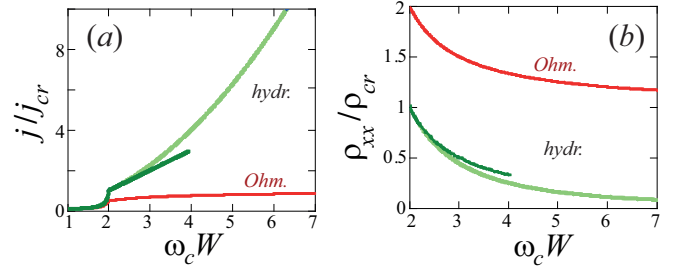


FIG. S8. Current (a) and longitudinal resistance (b) as functions of magnetic field near and far beyond the critical field $\omega_c^{cr} = 2/W$ for the ballistic-hydrodynamic and the ballistic-Ohmic phase transitions at the coinciding interparticle and disorder scattering rates: $\gamma_{ee} = \gamma' = \gamma$. Red curves for the Ohmic samples are plotted by formulas (S97). Dark green curves for j and ϱ_{xx} in the vicinity of the ballistic-hydrodynamic phase transition are drawn by formulas (S89) and (S93), which do not take into account the inhomogeneous distribution of central electrons. Light-green curves schematically show the results for the inhomogeneous hydrodynamic flow. The asymptote of light-green and red curves at $\omega_c \gg 1/W$ correspond to the bulk hydrodynamic (S99) and Ohmic (S100) resistances.

and E_H , as it was mentioned above, are valid at any relation between R_c and W .

At large magnetic fields, $\omega_c \gg 1/W$, in pure samples the hydrodynamic contribution from the central electrons to the current dominates. The averaged resistance is given by the formula: $\varrho_P = 12\eta_{xx}/W^2$ [17], where η_{xx} is the diagonal viscosity coefficient, being equal in our notations to $\eta_{xx} = \gamma/(16\omega_c^2)$ at $\gamma \ll \omega_c$. Thus, we obtain for the averaged sample resistance at $W \gg 1/\omega_c$:

$$\varrho_P(\omega_c) = \frac{3\gamma}{4\omega_c^2 W^2}. \quad (\text{S99})$$

In this formula we neglect the contribution from the edge electrons in the narrow near-edge regions $W/2 - |y| \gtrsim R_c$ [see Fig. 2(f) in the main text].

In the limit $\omega_c \gg 1/W$ for disordered samples we obtain from Ref. (S97) in the limit $W \gg R_c$ the usual Drude result for magnetoresistance of long samples, which is independent on ω_c :

$$\varrho_D(\omega_c) = \gamma'. \quad (\text{S100})$$

It is noteworthy that both the hydrodynamic and the Ohmic resistances ϱ_P and ϱ_D are proportional to the scattering rates γ and γ' , but the second one decreases with the magnetic field as $\sim 1/(\omega_c W)^2$. In Fig. S8 we schematically plot the dependencies $j(\omega_c)$ and $\varrho_{xx}(\omega_c)$ near and far from the transition ballistic-hydrodynamic and the ballistic-Ohmic transitions. At $0 < \omega_c W - 2 \ll 1$ these curves are described by Eq. (S89), (S93), (S97), and (S98). At $\omega_c \gg 1/W$ they follow the asymptotes ϱ_P (S99) and ϱ_D (S100).

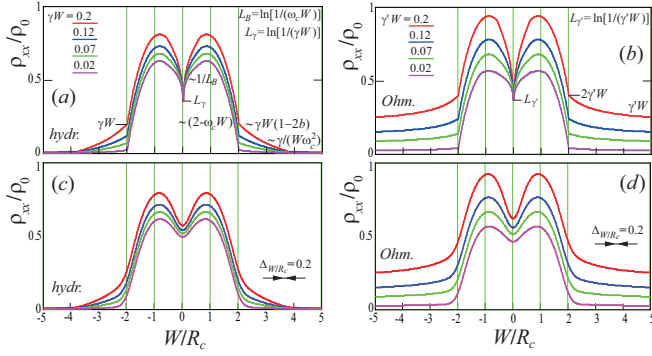


FIG. S9. Longitudinal ρ_{xx} resistance as functions of the parameter $W/R_c \propto B$, normalized on the nominal ballistic resistance $\rho_0 = m/(ne^2W)$, for pure samples at different intraparticle scattering rates γ (a,c) and for the disordered samples with no intraparticle scattering at different disorder scattering rates γ' (b,d). Curves in panels (c,d) are plotted by convolution of curves in panels (a,b), with a Gaussian with a width $\Delta_{W/R_c} = 0.2$, that qualitatively accounts sample imperfections.

In Fig. S9 we plot the longitudinal resistance $\rho_{xx}(B)$ in the whole interval of magnetic fields for a sample with no disorder at different interparticle scattering rates γ [panels (a,c)] and for a sample with no interparticle scattering at the same values of the scattering rate on bulk disorder γ' [panels (b,d)]. The results presented in Fig. S9 are a more precise and detailed version for of the results in Fig. S5. Curves in panels (a,b) are plotted by the interpolation formulas based of the presented above asymptotes for ρ_{xx} in the three ballistic subregimes (Sec. 2), in the upper and the lower vicinities of the transition point $B = B_c$ (Sec. 3.3), and in the bulk limit (Sec. 3.3). In panels (c,d) we plot the curves from panel (a,b), smoothed by convolution with a Gaussian weight function $G_\Delta(B)$ with a width $\Delta_{W/R_c} = 0.2$, that simulates the contribution of several sections of a long sample with varying widths and other imperfections.

The ballistic-hydrodynamic and the ballistic-Ohmic phase transitions can be distinguished in the experimental data, primarily, by the relationship between the value of the longitudinal resistance at the transition point $\rho_{xx}|_{\omega_c W=2}$ and in the limit of high magnetic fields $\rho_{xx}|_{\omega_c W \gg 1}$. For the ballistic-hydrodynamic transition, the latter value decreases up to zero as $1/B^2$ with increasing magnetic field [see Fig. S9(a)] and quickly becomes much less than $\rho_{xx}|_{\omega_c W=2}$, while for the ballistic-Ohmic transition the value $\rho_{xx}|_{\omega_c W=2}$ is twice the value $\rho_{xx}|_{\omega_c W \gg 1}$ [see Fig. S9(b)].

Of particular interest is the behavior of the Hall resistance $\rho_{xy}(B) = E_H/j$. First, we saw that the dependencies $\rho_{xy}(B)$ for both the ballistic-hydrodynamic and ballistic-Ohmic transitions coincide one with another [see Fig. S6(d)]. Second, above the transition point, $\omega_c > \omega_c^{ct}$, the function $\rho_{xy}(B)$ is identically equal to its “standard”

value $\rho_{xy}^{(0)} = B/n_0ec$, corresponding to the Ohmic regime at low temperatures. This result is obtained in the main order by the small parameters γW , $\gamma'W$ and the calculation of the corrections to this main part of ρ_{xy} by the powers of γW , $\gamma'W$ will apparently lead to corrections to the standard value $\rho_{xy} = \rho_{xy}^{(0)}$ at high field $\omega_c W \gg 1$. Such corrections was obtained Ref. [25] in numerical solution of the kinetic equation and were experimentally studied in Refs. [4, 16].

4. COMPARISON WITH PRECEDING THEORETICAL AND EXPERIMENTAL WORKS

4.1. Related theoretical works

In Ref. [25] a numerical solution of the kinetic equation (S2) was carried out for the same system as we studied in this work: 2D electrons in a long sample with rough edges and various rates of interparticle and disorder scattering. The kinks in the dependencies of the resistances ρ_{xx} and ρ_{xy} on magnetic field B at the transition point $B = B_c$ were obtained in [25] for the case when the scattering length is longer than the sample width. In Figs. S10(a,b) we cite the results of Ref. [25] for the sample with a very weak electron-electron scattering and the more substantial (but also weak) scattering of electrons on bulk disorder, corresponding the mean free paths $l = l_{MR}$ much longer than the sample width.

Although the authors of Ref. [25] discussed the emergence of the central electrons above B_c those do not scatter on the edges, they did not considered the peculiar electron dynamics in the regimes just below the transition [in the third ballistic region, $\gamma W B_c \ll B_c - B \ll B_c$, and in the semiballistic pre-transition region $0 < B_c - B \lesssim \gamma W B_c$] as well as the interaction between the edge and the central electrons just above the transition, $0 < B - B_c \ll B_c$. The shapes of the dependencies $\rho_{xx}(B)$ and $\rho_{xy}(B)$ obtained within our model for the ballistic-hydrodynamic and the ballistic-Ohmic transitions by analytical calculations are similar to the one obtained in Ref. [25] for the ballistic-Ohmic transition in the narrow samples, $W \ll 1/\gamma$ (see Fig. S10). Curves in Figs. S10(c,d) are plotted by the interpolation formulas based of the obtained above and cited above asymptotes for ρ_{xx} and ρ_{xy} in the three ballistic subregimes, in both the upper and the lower vicinities of the transition point $B = B_c$, and in the bulk limit $W \gg R_c$.

Note that the results for ρ_{xx} and ρ_{xy} in pure samples with long interparticle scattering lengths and no scattering on disorder, were not presented in Ref. [25], although, apparently, they could be calculated in the same method as was used in [25] for the obtaining of the resistances ρ_{xx} and ρ_{xy} in a disordered sample [see Figs. S10(a,b)]. In the current work we succeeded in obtaining the dependencies $\rho_{xx}(B)$ and $\rho_{xy}(B)$ in both the pure samples

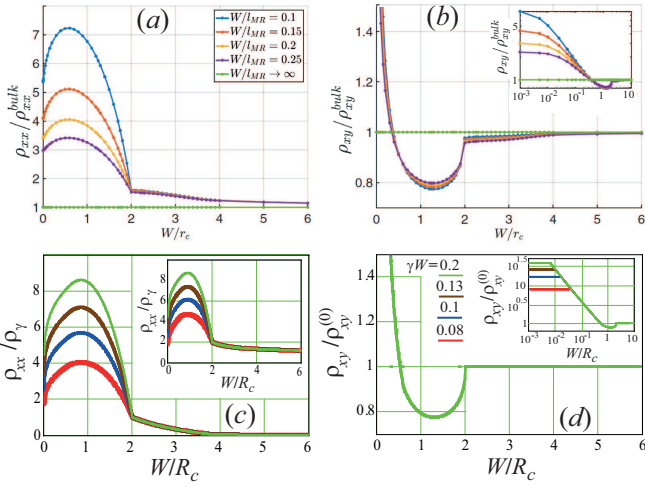


FIG. S10. Comparison of the results of the numeric solution of kinetic equation (S2) in Ref. [25] with the results of our analytical theory. Panels (a,b), taken from Ref. [25], show the longitudinal ρ_{xx} and the Hall ρ_{xy} resistances as function of magnetic field for the narrow samples, $W < l_{MR}$, the where scattering of 2D electrons on disorder dominates (l_{MR} is corresponding scattering length). Panels (c,d) present our results for ρ_{xx} and ρ_{xy} plotted in the same units as the ones in panels (a,b). Main graphics in panels (c,d) correspond to pure samples with only the interparticle scattering with several rates γ shown in panel (d). Inset in panel (c) present ρ_{xx} for disordered samples with no interparticle scattering and the disorder scattering rates γ' equal to the values γ used for the curves in main panel (c). Results for ρ_{xy} , shown in panel (d), are identical in the considered main approximation by γW for both pure samples and disordered samples at $\gamma = \gamma'$. Inset in panels (b) and (d) show the function $\rho_{xy}(B)$ in the logarithmic scales.

($\gamma \gg \gamma'$, $\gamma W \ll 1$) as well as of the disordered samples ($\gamma \ll \gamma'$, $\gamma' W \ll 1$) in an exact form in the limiting magnetic fields $B \ll B_c$ and $|B - B_c| \ll B_c$.

In Ref. [26] the ballistic and the hydrodynamic transport of 2D electrons in a long stripe was theoretically studied. In that work, similar general formula for the distribution function in the ballistic regime [Eq. (S20)] was obtained. Also the simplified form of the distribution function in the second ballistic subregime [Eq. (S27)] was derived and the resulting anomalously large Hall field, $E_H \sim E_0$, was deduced. Additionally a numeric description of the hydrodynamic-ballistic transport regime above the transition field at $\omega_c W - 2 \sim 1$, in particular, the detailed studies of the Hall field profiles, were performed.

In Ref. [26] the evolution of the dynamics of individual 2D electrons in a long sample with the increase of a magnetic field (in particular, the emergence of the edge and the central electrons at $\omega_c W > 2$) was generally discussed. However the curvature of the Hall field profile $E_H(y)$, characterizing the evolution of the type of a flow, was attracted the main attention, whereas the

presence of a genuine phase transition at $\omega_c W = 2$ between the ballistic almost independent electrons and a collectivized electron fluid phase as well as the nontrivial semi-ballistic dynamics of electrons in the first and third ballistic sub-regimes were not studied. In our work, we provide a proper description of the flow in the first and the third ballistic subregimes; explain the origin of the bulk contribution to the Hall resistance $\rho_{xy} = \rho_{xy}^0/2$ in the limit $B \rightarrow 0$; as well as reveal and study the ballistic-hydrodynamic and the ballistic-Ohmic phase transitions at $\omega_c W = 2$.

To conclude this section, we note that the mean field model developed in Sections 3.2 and 3.3, apparently, has the usual accuracy of the methods of this type, namely, describes all quantities in the vicinities of the phase transition up to numerical factors of the order of unity. Such description of the phase transition within the basic equations of Sec. 1, apparently, can be refined only by numerical calculations similar to the ones performed in Refs. [25, 26]. However, the collision operator (S3), used in this work and in [25, 26] is already a significant simplification of the exact operator of electron-electron collisions. For example, even for the 2D electron systems with the simplest quadratic electron spectrum, like GaAs quantum wells, the relaxation rates γ_m of the distributions proportional to various harmonics $e^{im\varphi}$ have different orders of magnitudes [30], in contrast to operator (S3) leading to the same relaxation rates, γ , of the second and the all higher harmonics.

We also remind that the proposed mean field model may be considered as the application of the additionally simplified form St' (S74) of the electron-electron collision operator St (S3). Collision operator (S74) does not take into account the spatial peculiarities of the flow, but seems to be sufficient for a qualitative description of the average characteristics of the flow and their dependencies on magnetic field.

4.2. Related experiments

In this subsection we compare the results of experiments [5, 6, 9–11, 15] with our results on the ballistic-hydrodynamic phase transition and on the magnetoresistance in different regimes.

In Ref. [5] a flow of 2D electrons in a graphene stripe was experimentally studied. Magnetoresistance and distributions of the Hall electric field over the cross section of the stripe were measured at various magnetic fields, electron densities, and temperatures corresponding to the ballistic and the hydrodynamic regimes. The obtained experimental dependencies $\rho_{xx}(B)$ are very similar to the theoretical ones presented in Figs. S5(a) and S9. In Fig. 3 in the main text we cite the magnetoresistance curves measured in Ref. [5] and present our theoretical results for reasonable values of the parameter γW .

Both the experimental and the theoretical dependencies $\rho_{xx}(B)$ exhibit a positive magnetoresistance at $B \ll B_c$, a nonmonotonous behavior at $B \lesssim B_c$ with a maximum at $B \sim B_c/2$, a smeared kink at the critical field $B = B_c$, the dependence similar to $\rho_{xx}(B) - \rho_{xx}(B_c) \sim B_c - B$ at $0 < B_c - B \ll B_c$, and a monotonous decrease at $B > B_c$. This coincidence signifies that the ballistic sub-regimes and the ballistic-hydrodynamic phase transition, theoretically revealed in our work, were apparently realized and observed in experiment [5].

In Ref. [6] an observation of the profile of the current density $j(y)$ for a flow of 2D electrons in a graphene stripe was performed by measurements of the local magnetic field induced by the distribution of $j(y)$. Additionally, magnetoresistance of a graphene stripe, being very similar to the magnetoresistance reported Ref. [5], was observed. In Fig. 3(b) in the main text we cite the magnetoresistance curves presented in Supplemental information of Ref. [6]. These curves exhibit a well-pronounced kink at $B = -B_c$, a maximum at $B \sim \pm B_c$, and the behavior $\rho_{xx}(|B|) - \rho_{xx}(B_c) \sim B_c - |B|$ at $0 < B_c - |B| \ll B_c$. The kink at the critical field $B = B_c$, apparently indicating the phase transition, is observed in [6] more clearly, than in [5]. Note that the dependencies $\rho_{xx}(B)$ from Ref. [6] are substantially asymmetric by $B \rightarrow -B$ [see Fig. 3(b) in the main text]. The last fact can be related with an admixture of the Hall resistance in the observed resistance. This is especially clearly evidenced by the asymmetry of the kink at $B = \pm B_c$.

In Ref. [5] the Hall field profiles $E_H(y)$ were measured in a most part, but not in the entire section of each studied stripe. In the ballistic regime these profiles turned out to be nearly flat, while in the hydrodynamic regimes they were strongly curved, similarly to the parabolic hydrodynamic profiles corresponding to the Poiseuille flow. Based on our theoretical results, we predict that the sharp features in $E_H(y)$ near the sample edges, $y = \pm W/2$, can be observed at $B < B_c$ in future studies similar to experiment [5], provided the profiles $E_H(y)$ will be measured up to the very sample edges. The divergent features in $E_H(y)$ were obtained in our theory for all three ballistic subregimes, however they have largest width and amplitude in the lower vicinity of B_c [see Fig. S4 and Fig. 2 in the main text]

In Ref. [16], a flow of 2D electrons in long samples of high-quality GaAs quantum wells was experimentally studied. The dependencies of the resistances ρ_{xx} and ρ_{xy} on magnetic field were measured. We cite these results of Ref. [16] in Figs. S11(a,b). Apparently, in the 2D electron system studied in Ref. [16] the ballistic transport regime at $W < 2R_c$ and the hydrodynamic regime at $W > 2R_c$ were realized. The experimental dependencies $\rho_{xx}(B)$ is rather similar to the magnetoresistance observed in Refs. [5, 6] in graphene stripes and to our theoretical result for $\rho_{xx}(B)$ presented in Fig. S5(a) and S9. The experimental result of Ref. [16] for $\rho_{xy}(B)$ is also rather

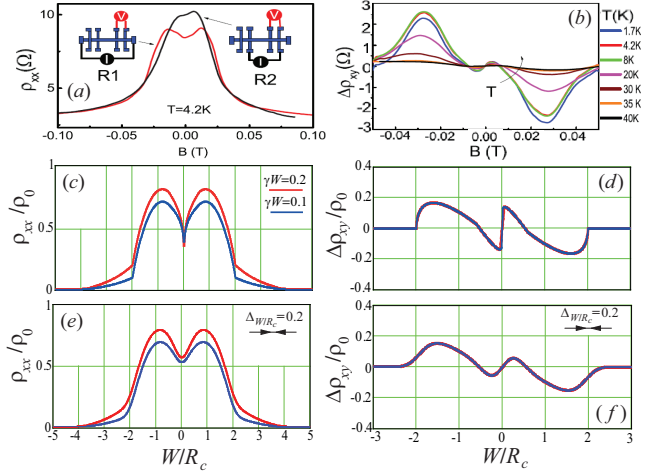


FIG. S11. Longitudinal ρ_{xx} and Hall resistances ρ_{xy} of long GaAs quantum wells samples [in panels (b,d,f) the value $\Delta\rho_{xy} = \rho_{xy} - \rho_{xy}^{(0)}$ is drawn]. Panels (a,b) present the experimental results of Ref. [16]. Panels (c,d) show our results for ρ_{xx} and ρ_{xy} for pure long samples with no disorder and the two values of the interparticle scattering rates γ . In panels (e,f) we plot the curves from panel (a,b), smoothed by convolution with a Gaussian weight function $G_\Delta(B)$ with a width Δ_{W/R_c} , that simulates the contribution of several sections of a long sample with varying widths as well as other sample imperfections. The magnetic fields 0.05 T at the right and the left edges of panel (b), where the resistance ρ_{xy} becomes close to the standard value $\rho_{xy}^{(0)}$, well correspond to the equality $2R_c \approx W$, where $W = 5 \mu$ is the width of the sample studied in Ref. [16].

similar to the theoretical one obtained in the current work [see Fig. S5(b)]: the curve $\rho_{xy}(B)$ exhibits positive and negative deviations from the standard Hall resistance $\rho_{xy}^{(0)} = B/(n_0ec)$ below the transition point, $W < 2R_c$, and an almost exactly coincidence with $\rho_{xy}^{(0)}$ above the transition point, $W > 2R_c$. In Figs. S11(c,d) we plot the dependencies $\rho_{xx}(B)$ and $\Delta\rho_{xy}(B) = \rho_{xy}(B) - \rho_{xy}^{(0)}(B)$ obtained by the interpolation of the obtained and cited above asymptotes of these functions in the limiting diagrams of B , as it was done in Figs. S9 and S10.

It is noteworthy that the magnitude and the sharpness of the features of $\rho_{xx}(B)$ and $\rho_{xy}(B)$ observed in Ref. [16] at $\omega_c W \lesssim 2$ are smaller than the ones observed for ρ_{xx} in Refs. [5, 6]. This can be associated with a larger magnitude of imperfections of the samples of Ref. [16] as compared with the graphene stripes examined in Refs. [5, 6]. In Figs. S11(e,f) we plot the curves $\rho_{xx}(B)$ and $\rho_{xy}(B)$ from panel (c,d), smoothed by convolution with a Gaussian weight function with a width $\Delta_{W/R_c} = 0.2$, that simulates the contribution of several sections of a long sample with varying widths, the samples corners, and other imperfections. It is seen that the curves in panels (e,f) much better fit the experimental curves in panels (a,b), than the ones in panels (c,d).

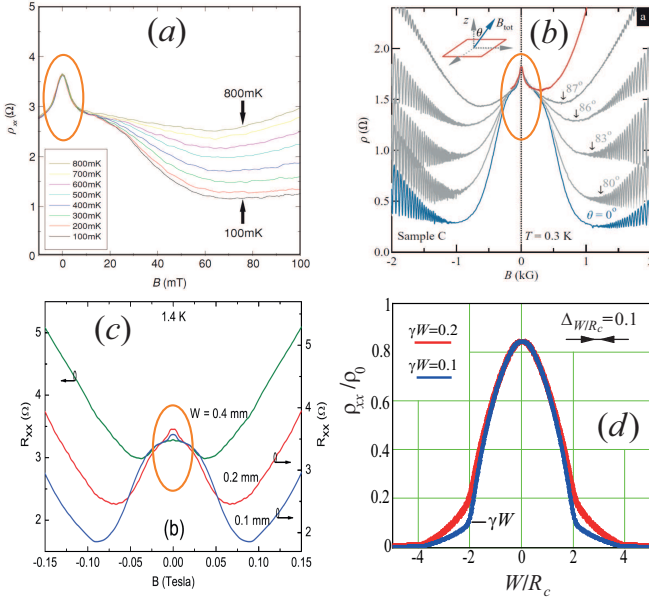


FIG. S12. (a-c) Longitudinal “bell-shape” magnetoresistance of high-mobility GaAs quantum wells at low temperatures. Panels (a,b,c) are taken from experimental articles [9],[10],[11], respectively. In the samples studied in Ref. [9] (and possibly, in others) macroscopic defects present, which divide the 2D electron flow in the sample on subregions of smaller sizes. Apparently, in all experiments [9]–[11] the effective length and width of the sample subregions were comparable one with other, being much smaller than the interparticle scattering length and the length of the scattering on other disorder. In panel (d) we plot the ballistic-hydrodynamic magnetoresistance given by Eqs. (S46) and (S93), obtained within our model for the case of short samples with $W \sim L \ll l$. The curves are smoothed by convolution with a Gaussian weight function $G_{\Delta}(B)$ with a width $\Delta W/R_c$ in order to take into account the contributions from several sample subregions.

We conclude that the predicted magnetic field dependencies of the longitudinal and of the Hall resistances $\rho_{xx,xy}(B)$ in the ballistic subregimes as well as around and far above the ballistic-hydrodynamic phase transition are in a good agreement with results of experiments [5, 6, 16].

Additionally, we analyze experiments [9–11] on magnetotransport of 2D electrons in high-mobility GaAs quantum wells. In Figs. S12(a-c) we cite the magnetoresistance measured in those works. Apparently, the observed negative magnetoresistance in the very low magnetic fields has a purely ballistic origin. Indeed, it is independent on temperature [see Fig. S12(a)]; is robust to the effect of in-plane magnetic field [see Fig. S12(b)]; and occurs in sufficiently narrow samples [see Fig. S12(c)].

We argue that such negative magnetoresistance is qualitatively explained by our result (S46) obtained for the first ballistic subregime in the case of the short samples, $W \sim L \ll l$. We remind that formula (S46) originates from the bending of the ballistic trajectories of the

travelling electrons, leading on the increase their average length [28]. Similar negative ballistic magnetoresistance (S45) is also possible in long samples at $\omega_c \ll \gamma^2 W$, when the effect of the near-edge layers with the skipping is suppressed [the small orange peak near $B = 0$ in Fig. S5(a)]. However, in the narrow samples such magnetoresistance is much more pronounced and therefore can be more easily observed.

Due to the presence of the macroscopic oval defects in the samples examined in Ref. [9] (see details in Ref. [13]) and, possibly, in Refs. [10, 11], the characteristic width and length of the flows can differ from W and L of those samples. Such effective width W_{eff} is to be of the order of the mean distance between the oval defects and becomes smaller than W (see discussions in Refs. [17],[28]). In this case, the purely ballistic regime is realized when the cyclotron diameter $2R_c$ and the bulk scattering length l , related to the scattering on other disorder and/or interparticle collisions, are larger than the effective width W_{eff} and length L_{eff} . At $W_{eff} \sim L_{eff}$, the ballistic negative magnetoresistance (S46) should appear at $\omega_c \ll 1/W_{eff}$, unlike the case of long stripes, in which such magnetoresistance is realized in the subregimes $\omega_c \ll \gamma^2 W$ or $\omega_c \ll W/L^2$ (see Sec. 2.3).

Our estimates shows that the temperature-independent negative magnetoresistance in Figs. S12(a-c) occurs in the magnetic fields $B \ll B_c^{eff}$, where B_c^{eff} corresponds to the cyclotron radius R_c of the order of the mean distances between the oval defects and, thus, of the effective width W_{eff} (see Ref. [28] for details). In the larger magnetic fields, $B \sim B_c^{eff}$, a smeared ballistic-hydrodynamic transition is to be realized by the mechanism similar to the one studied in Sec. 3 for the long samples (see also the discussion in the end of Sec. 3.2). At $B \gg B_c^{eff}$ the hydrodynamic temperature-dependent magnetoresistance arises due to the formation of a viscous flow.

Finally, we note that the sharp ballistic-hydrodynamic transition in 2D electron flows can be possibly realized not only in stripes, but also in the bulk samples similar to the discussed above GaAs quantum wells with oval defects, but containing thermodynamically large numbers of such defects. Magnetotransport in such systems was theoretically considered in many works without taking into account the hydrodynamic effects (see, for example, Refs. [32–35]). Accounting for the interparticle collisions, apparently, should lead to the realization of the hydrodynamic regime at the magnetic fields B larger than some exact critical field B_c^{bulk} , corresponding to the cyclotron radius of the order of the mean distance between the defects and, additionally, to the formation of a connected region (“cluster”) with the 2D fluid nucleus. The description of such ballistic-hydrodynamic phase transition is to require more complex methods than the ones used in this work, first of all, the percolation theory.